Numerical model to determine the composition of H_2O-NaCl-$CaCl_2$ fluid inclusions based on microthermometric and microanalytical data

M. Steele-MacInnis[1], R. J. Bodnar[1] and J. Naden[2]

[1.] Department of Geosciences, Virginia Tech, Blacksburg, VA 24061

[2.] British Geological Survey, Keyworth, Nottingham UK NG12 5GG

REVISED MANUSCRIPT W7363

Submitted August 13, 2010

Abstract

Natural fluids approximated by the H_2O-NaCl-$CaCl_2$ system are common in a wide range of geologic environments, including sedimentary basins associated with hydrocarbon occurrences and MVT deposits, submarine hydrothermal systems, and other metamorphic, magmatic and hydrothermal environments. We present a comprehensive numerical model and Microsoft® Excel©-based computer program to determine the compositions of fluid inclusions in the H_2O-NaCl-$CaCl_2$ system based on microthermometric and microanalytical data. The model consists of six polynomial correlation equations that describe liquid salinity as a function of NaCl/$CaCl_2$ ratio and melting temperature on each of the ice, hydrohalite, halite, antarcticite, $CaCl_2 \cdot 4H_2O$ and $CaCl_2 \cdot 2H_2O$ vapor-saturated liquidus surfaces. The cotectic and peritectic boundaries are determined from the intersections of the liquidus surfaces. The model is implicitly internally consistent and topologically correct.

The model expands upon the compositional range of applicability and the data types that can be used for compositional determination. It reproduces experimental data for all compositions that lie within the H_2O-NaCl-$CaCl_2 \cdot 4H_2O$ compositional triangle in the H_2O-NaCl-$CaCl_2$ system and yields accurate reproductions of the H_2O-NaCl and H_2O-$CaCl_2$ binaries. Furthermore, in comparison to previously published models, the one presented here eliminates systematic errors, wavy isotherms and cotectic and peritectic curves with local “bumps.”

List of Symbols

n_i	number of moles of component *i*
X_i	Mole fraction of component *i* [= $(n_i)/(n_{total})$]
Ψ	The molar fraction of NaCl relative to NaCl + $CaCl_2$ [= $(X_{NaCl})/(X_{NaCl} + X_{CaCl2})$]
Φ	The weight fraction of NaCl relative to NaCl + $CaCl_2$ [= (wt.% NaCl)/(wt.% NaCl + wt.% $CaCl_2$)]
Ω	The molar fraction of $CaCl_2$ relative to H_2O + $CaCl_2$ [= $(X_{CaCl2})/(X_{CaCl2} + X_{H2O})$]
$T_{m,x}$	Temperature (°C) at which solid phase *x* melts on the one-solid-stable vapor-saturated liquidus surface.
$T_{pb,x}$	Temperature (°C) at which solid phase *x* melts on either a cotectic or peritectic phase boundary curve, in the presence of liquid plus vapor plus another solid. Subscripts *x: ice* (= H_2O solid)*; hh* (= hydrohalite); *h* (= halite); *ant* (= antarcticite); *Ca4h* (tetrahydrate = $CaCl_2 \cdot 4H_2O$); *Ca2h* (dihydrate = $CaCl_2 \cdot 2H_2O$ = sinjarite)
S_{mol}	Total salinity on a mole fraction basis [= $X_{NaCl} + X_{CaCl2}$].
S_{wt}	Total salinity on a wt.% basis [= (wt.% NaCl + wt.% $CaCl_2$)]
a_i	Regression coefficient.

Introduction

Aqueous fluids in which NaCl and $CaCl_2$ are the two most abundant salts and which may be adequately described by the system H_2O-NaCl-$CaCl_2$ are common in many geologic environments. Fluids of this composition are commonly found in sedimentary basins (COLLINS, 1975; LOWENSTEIN et al., 2003; HANOR and MACINTOSH, 2007), Mississippi Valley-Type Pb-Zn deposits (HAYNES and KESSLER, 1987; BASUKI and SPOONER, 2002; STOFFELL et al., 2008), Archean lode gold deposits (ROBERT and KELLY, 1987), skarn and greisen deposits (KWAK and TAN, 1981; LAYNE and SPOONER, 1991; SAMSON et al., 2008), iron-oxide Cu-Au (IOCG) -type deposits (XU, 2000), magmatic Cu-Ni deposits (LI and NALDRETT, 1993), crystalline rocks of the Canadian Shield (FRAPE et al., 1984), mafic pegmatoids associated with platinum deposits in the Bushveld Complex (SCHIFFRIES, 1990) and elsewhere (NYMAN et al., 1990), and in sub-seafloor hydrothermal systems (VANKO, 1988; VANKO et al., 1988). Thus, fluid inclusions approximated by the system H_2O-NaCl-$CaCl_2$ are common in a diverse range of geologic environments, and a methodology to interpret microthermometric data obtained from these inclusions is necessary to better understand geologic processes such as diagenesis, hydrocarbon migration, evolution of hydrothermal systems, metal transport, metamorphism and crystallization of magmas.

The best source of information concerning the compositions of paleo-geologic fluids comes from fluid inclusions (ROEDDER, 1984). The temperatures at which phase changes occur within a fluid inclusion during heating can be used to estimate the fluid composition, assuming that PTX phase relationships of representative fluid systems are available. In addition, the elemental ratios in saline aqueous inclusions can be determined by microanalysis, for example by laser ablation ICPMS (LA-ICPMS) (GÜNTHER et al., 1998), which provides an additional constraint for determining the fluid composition when combined with microthermometric data.

The system H_2O-NaCl-$CaCl_2$ (Fig. 1) is a three-component system, and the phase rule requires that two variables must be specified to determine a unique liquid composition on the vapor-saturated liquidus, whereas one variable is sufficient to determine a unique liquid composition on any vapor-saturated, two-solid-plus-liquid boundary (cotectic or peritectic curve). The temperatures of last melting of solid phases, either on a cotectic or peritectic curve ($T_{pb,x1}$) or on the one-solid liquidus ($T_{m,x2}$), are two possible sources of data; elemental ratios determined from LA-ICPMS represent another data source. (Note that whereas several previous studies of the H_2O-NaCl-$CaCl_2$ system have used the term "X_{NaCl}" to refer to the weight ratio of NaCl relative to NaCl+$CaCl_2$, we adopt the more common notation such that X_{NaCl} refers to the mole fraction of NaCl, and we instead denote the weight and molar ratios of NaCl relative to NaCl+$CaCl_2$ as Φ and Ψ, respectively). As discussed in detail below, depending upon which data are available, fluid inclusion compositions may be determined using a combination of either the temperature of melting on a cotectic or peritectic *and* a temperature of melting on the vapor-saturated liquidus surface ($T_{pb,x1} + T_{m,x2}$), or a temperature of melting on the vapor-saturated liquidus surface *and* the ratio of the amount of NaCl relative to the total amount of NaCl and $CaCl_2$, ($T_{m,x}$ + either Φ or Ψ – the two compositional ratios can be directly converted to one another via the molar masses of the species) or the temperature of melting of one phase on a cotectic or peritectic *and* the temperature of melting of a second phase on a cotectic or peritectic ($T_{pb,x1} + T_{pb,x2}$).

Compositions of H_2O-NaCl-$CaCl_2$ fluid inclusions can be approximated using graphically-displayed phase equilibrium data (e.g., KONNERUP-MADSEN, 1979; ROBERT and KELLEY, 1987) or using empirical or theoretical data (OAKES et al., 1990; WILLIAMS-JONES and SAMSON, 1990; NADEN, 1996; CHI and NI, 2007), and several computer packages have been

developed to interpret data from fluid inclusions whose compositions are approximated by the system H_2O-NaCl-$CaCl_2$ (NADEN, 1996; BAKKER, 2003; CHI and NI, 2007). While each model works well over a limited range of T-X conditions, none of the currently available models is equipped to calculate fluid inclusion compositions over the complete range in compositions reported for natural H_2O-NaCl-$CaCl_2$ fluid inclusions. Moreover, some of the previously published equations (OAKES et al., 1990; NADEN, 1996; CHI and NI, 2007) are characterized by structured residuals with respect to the experimental data, or have inflections ("bumps") between data points and local extrema along calculated isotherms and univariant curves, as described in more detail below. Finally, none of the previously published models provide the ability to determine fluid compositions using the complete range of possible input data, such as the temperature of melting on a cotectic or peritectic *and* a temperature of melting on the vapor-saturated liquidus surface ($T_{pb,x1} + T_{m,x2}$), or a temperature of melting on the vapor-saturated liquidus surface *and* the weight fraction of NaCl relative to NaCl + $CaCl_2$ ($Tm_{,x} + \Phi$), or the temperature of melting of one phase on a cotectic or peritectic *and* the temperature of melting of a second phase on a cotectic or peritectic ($T_{pb,x1} + T_{pb,x2}$), as described below. The model presented here incorporates those aspects of previous models that have been shown to be consistent with the phase equilibria determined from experimental data, and adds new equations and methods to expand the T-X range of applicability, remove anomalies inherent in some previous statistical models, and expands the range of input data that may be used to estimate the composition of H_2O-NaCl-$CaCl_2$ fluid inclusions.

The goal of this study is to provide a comprehensive set of empirical equations that describe the portion of the vapor-saturated H_2O-NaCl-$CaCl_2$ system that includes the range of compositions of natural fluid inclusions and the range of available experimental data. As such,

this study covers a region within the ternary system bounded by the H_2O apex, the NaCl apex and the composition of $CaCl_2 \cdot 4H_2O$ on the H_2O-$CaCl_2$ binary (Fig. 1b). The equations derived in this study have been assembled into a Microsoft® Excel©-based program to allow users to easily calculate fluid inclusion compositions in this complex system over the complete compositional range reported from natural fluid inclusions, using a variety of input data, including $T_{pb,x1} + T_{m,x2}$, $T_{m,x} + \Phi$ or $T_{pb,x1} + T_{pb,x2}$. The program is available as an electronic annex to this paper.

We emphasize that the model developed in this study applies to stable equilibrium melting behavior in the system H_2O-NaCl-$CaCl_2$, but metastable melting phenomena are also frequently encountered in $CaCl_2$-bearing fluids (e.g., POTTER and CLYNNE, 1978; ROEDDER, 1984; VANKO et al., 1988; BAUMGARTNER and BAKKER, 2009). For instance, VANKO et al. (1988) reported that some of their synthetic H_2O-NaCl-$CaCl_2$ fluid inclusions could not be completely frozen, while others could only be frozen to a metastable phase assemblage. Likewise, LINKE (1958) and BAUMGARTNER and BAKKER (2009) report the occurrence of several metastable phase assemblages in the H_2O-$CaCl_2$ binary system. While we acknowledge that metastable behavior in the H_2O-NaCl-$CaCl_2$ system does occur, the model presented in this study specifically represents only the *stable* phase relations on the vapor-saturated H_2O-NaCl-$CaCl_2$ liquidus.

Vapor-Saturated Phase Relations in the H_2O-NaCl-$CaCl_2$ System

Phase relations on the vapor-saturated liquidus of the H_2O-NaCl-$CaCl_2$ ternary system are shown in Figure 1. The system is characterized by at least eight fields in which a single solid phase is in equilibrium with liquid and vapor. Six of these fields are described in this study; two additional fields in the high salinity, $CaCl_2$-rich, low weight fraction NaCl (Φ) part of the system (near the $CaCl_2$ apex; Fig. 1a) are not considered here because experimental data are not

available in that part of the ternary system (although these phases have been characterized along the H_2O-$CaCl_2$ binary, e.g. LINKE, 1958). Figure 1 shows phase relationships in the part of the system that includes the range of reported compositions of natural fluid inclusions. The phase boundaries shown in Figure 1c were calculated using the equations derived in this study and below we compare these calculated phase boundaries with experimental data.

Each field shown in Figure 1 is labeled according to the solid phase that is in equilibrium with liquid and vapor. At low salinity, near the H_2O apex, the stable solid phase on the liquidus surface is H_2O ice (Fig. 1a, c). At intermediate to high salinity and $R_{wt} > 0.04$, halite (NaCl) is the stable solid phase (Fig. 1a, c). A field in which hydrohalite ($NaCl \cdot 2H_2O$) is the stable solid phase separates the ice- and halite-stable fields (Fig. 1a, c). At intermediate to high salinity and $R_{wt} < 0.04$, calcium chloride hydrates are the stable solid phases: antarcticite ($CaCl_2 \cdot 6H_2O$) is the stable phase from about 30 to 50 wt.% total salt, "tetrahydrate" ($CaCl_2 \cdot 4H_2O$) is the stable solid from 50 to about 57 wt.% salt, and "dihydrate" ($CaCl_2 \cdot 2H_2O$ = sinjarite) is stable from about 57 to 75 wt.% salt (Fig. 1a, c). To our knowledge, ternary experimental data are not available for the H_2O-NaCl-$CaCl_2$ system at salinities above 75 wt.% total salt, thus the $CaCl_2 \cdot H_2O$ and $CaCl_2$ (anhydrous) stable fields are not included in this study (area near the $CaCl_2$ apex on Fig. 1a labeled with a question mark, ?). Also shown in Figure 1c are the compositions of hydrohalite (61.86 wt.% NaCl on the H_2O-NaCl binary), antarcticite (50.07 wt.% $CaCl_2$ on the H_2O-$CaCl_2$ binary), $CaCl_2 \cdot 4H_2O$ (60.63 wt.% $CaCl_2$ on the H_2O-$CaCl_2$ binary) and $CaCl_2 \cdot 2H_2O$ (75.49 wt.% $CaCl_2$ on the H_2O-$CaCl_2$ binary).

The fields in which one solid is in equilibrium with liquid and vapor are separated from each other by peritectic or cotectic boundary curves. Ice and hydrohalite are separated by the ice + hydrohalite (I+HH) cotectic, which extends from the ternary eutectic point (E) at -52°C

(YANATIEVA, 1946) to the binary H_2O-NaCl eutectic (E') at -21.2°C (HALL et al., 1988). Ice and antarcticite are separated by the ice + antarcticite (I+A) cotectic, which extends from the ternary eutectic (E) to the binary H_2O-$CaCl_2$ eutectic (E") at -49.8°C (YANATIEVA, 1946). The hydrohalite and antarcticite fields are separated from each other by the hydrohalite + antarcticite (HH+A) cotectic curve, which extends from the ternary eutectic (E) to the first ternary peritectic (P_1) at -22.4°C (YANATIEVA, 1946). The hydrohalite field is separated from the halite field by the hydrohalite + halite (HH+H) peritectic curve, which extends from the first ternary peritectic (P_1) to the binary H_2O-NaCl peritectic (P') at +0.1°C (LINKE, 1958). The halite field is separated from the antarcticite field by the halite + antarcticite (H+A) cotectic curve, which extends from the first ternary peritectic (P_1) to the second ternary peritectic (P_2) at +29°C (SCHIFFRIES, 1990). The halite field is separated from the tetrahydrate field by the halite + tetrahydrate (H+Ca4h) cotectic, which extends from the second ternary peritectic (P_2) to the third ternary peritectic (P_3) at approximately +45°C (estimated from the data of LINKE, 1958). The halite field is separated from the dihydrate field by the halite + dihydrate (H+Ca2h) cotectic curve, which extends from the third ternary peritectic (P_3) to the fourth ternary peritectic at >110°C (LINKE, 1958). The antarcticite field is separated from the tetrahydrate field by the antarcticite + tetrahydrate (A+Ca4h) peritectic curve, which extends from the second ternary peritectic point (P_2) to the first binary H_2O-$CaCl_2$ peritectic (P_1") at +30.1°C (LINKE, 1958). Tetrahydrate is separated from dihydrate by the tetrahydrate + dihydrate (Ca4h+Ca2h) peritectic curve, which extends from the third ternary peritectic point (P_3) to the second binary H_2O-$CaCl_2$ peritectic (P_2") at +45.1°C (LINKE, 1958). The locations of other boundary curves that occur at higher salinity conditions close to the H_2O-$CaCl_2$ binary and near the $CaCl_2$ apex are not known. A detailed summary of

the stable melting paths followed by H_2O-NaCl-$CaCl_2$ fluid inclusions having compositions in the various fields described above is provided in Appendix A.

Sources of Experimental Data

The experimental data used in the regression analysis are summarized in Table 1 and Figure 2.

Phase Boundaries

Phase boundaries on the vapor-saturated liquidus in the system H_2O-NaCl-$CaCl_2$ are broadly characterized by either cotectic relationships or peritectic relationships. Note that on a cotectic boundary, the phase change behavior that is observed upon heating is always "solid1+solid2→solid2+liquid →liquid", whereas on a peritectic boundary, the reaction observed upon heating is "solid1+liquid→solid2+liquid→liquid". In other words, as a fluid inclusion is heated, the inclusionist would observe two solids shrinking (melting) along a cotectic curve until one disappeared leaving behind the second solid and liquid, whereas s/he would observe one solid growing at the expense of the other along a peritectic curve.

In addition to the T-X data along the cotectic and peritectic phase boundaries summarized in Table 1 and Figure 2, SCHIFFRIES (1990) reported the temperature at the second peritectic point (P_2) of +29°C, which provides an additional constraint on the location of the A+Ca4h, A+H and Ca4h+H phase boundary curves.

Liquidus Surfaces

In addition to compositions that lie on each divariant liquidus surface, data for the univariant boundary curves (peritectics or cotectics) adjacent to the surface were included in the regression for each liquidus surface. For example, in modeling the hydrohalite field, data from

the I+HH, HH+A and HH+H phase boundaries were used in addition to the hydrohalite-only liquidus data. For each liquidus field, the number of data points that have been used in the regression, including data within the field and those on the phase boundary curves, are listed in Table 1.

For the halite liquidus, the high temperature data of CHOU (1987) were omitted from the regression analysis, but these data are in excellent agreement with those of STERNER et al. (1988). In addition, the experimental data analyzed in this study include several liquidus temperature measurements along the anhydrous NaCl-$CaCl_2$ binary (ZHANG et al., 1995), but those data are not included in the data set for regression.

For the tetrahydrate liquidus, LINKE (1958) reports multiple polymorphs of $CaCl_2 \cdot 4H_2O$ coexisting with different salinity liquids. We have followed the suggestion of POTTER and CLYNNE (1978), who point out that consideration of the phase rule indicates that the "beta" and "gamma" polymorphs are metastable, and so we have included only the "alpha" polymorph solubility data of LINKE (1958).

Equations Describing the Liquidus and Phase Boundary Curves

The liquidi in a ternary system are divariant surfaces, and thus the total salinity (S_{wt}) can be represented as a function of the weight fraction of NaCl relative to NaCl + $CaCl_2$ (Φ) and the temperature of melting of the last solid phase on the vapor-saturated liquidus ($T_{m,x}$). The cotectic and peritectic curves are univariant lines and therefore both Φ and S_{wt} can be represented as a function of the temperature of melting of solid phase *x* on the cotectic or peritectic ($T_{pb,x}$). Previous studies have generally approached the problem of regression modeling of the vapor-saturated liquidi of ternary systems by fitting separate univariant regression equations to the experimental data on the phase boundary curves (e.g., STERNER et al., 1988; NADEN, 1996).

While that approach often produces a system of equations with small errors with respect to the experimental data, it also generally yields a model that is not internally consistent because predicted phase boundary curves will not necessarily intersect at the invariant points (eutectic and peritectic points) and predicted isotherms of adjacent fields will not always intersect at the univariant curves as they should. The approach taken in this study has been to regress the data for each liquidus surface, and weight the cotectic and peritectic curve appropriately to ensure that univariant curves represent the intersection of the adjacent liquidus surfaces. This approach has two advantages: First, it yields a model that is implicitly internally consistent, and secondly, it provides additional constraints on liquidus fields that are represented by sparse experimental data. For example, the only data available for the tetrahydrate field are along the H_2O-$CaCl_2$ binary (as described above). However, isotherms are available at the intersections of the tetrahydrate field with the adjacent antarcticite, halite and dihydrate fields, and these data, combined with data along the H_2O-$CaCl_2$ binary, provide reasonable constraints on the locations of isotherms within the tetrahydrate field.

Regression analyses were conducted using SAS© JMP 8 statistical software. The experimental data on each liquidus surface were regressed to find the equation that best satisfied three criteria: First, the equation was required to accurately reproduce the experimental data; secondly, the resulting isotherms were required to be smooth and monotonic, meaning free of local extrema and inflections; and thirdly, the equations for adjacent liquidus surfaces were required to intersect such that the cotectic and peritectic phase boundaries predicted by the intersection were consistent with experimental data. The percent residuals of each equation with respect to the experimental data were calculated by the expression {(1 - calculated/measured)*100%}.

Ice field

Salinities of fluid inclusions for which H_2O ice is the final solid to melt are described by the following equation, modified from NADEN (1996):

$$S_{wt} = \sum_{i=0}^{5} a_i T_{m,ice}^{i} + \sum_{i=6}^{7} a_i \Phi^{(i-5)} + a_8 \Phi\ T_{m,ice}^{2} + a_9 \Phi\ T_{m,ice}^{5} - 0.185 \exp(-T_{m,ice} - 52) \quad (1)$$

where $T_{m,ice}$ is the final ice melting temperature in degrees Celsius and the a_i's are fitting parameters given in Table 2. We have added the exponential term at the end of the equation originally provided by NADEN (1996) to improve the intersection with the antarcticite field, as discussed below. The equation for the ice liquidus surface of CHI and NI (2007) (their Eqn. (4)) is based upon extrapolation from their I+HH boundary, and is therefore valid only at high salinity ($T_{m,ice} \leq$ -21°C), and it shows significant structure in the residuals as a function of salinity (Fig. 3). The equation of OAKES et al. (1990) (their Eqn. (2)) fits the data well at salinities from 0 to 25 wt. %, but provides a poorer fit to the higher salinity data of YANATIEVA (1946), with a negative-sloped, apparently linear structure in the residuals in this range (Fig. 3). Equation (1) does not reproduce the lowest salinity experimental data as well as the equation of OAKES et al. (1990), but it provides a better fit in general over the entire salinity range of the ice field (Fig. 3). For these reasons, Eqn. (1) is recommended as the general equation for the ice field, and is adopted for all figures and examples herein, while the equation of OAKES et al. (1990) may be preferable if all data to be analyzed have a $T_{m,ice} \geq$ -15°C. The numerical model described later offers users the option to select the equation of OAKES et al. (1990) if their microthermometric data are in the range in which that model predicts values that are in better agreement with experimental values.

Hydrohalite field

The salinity of fluid inclusions in which hydrohalite is the final solid phase to melt is described by:

$$S_{mol} = \sum_{i=0}^{2} a_i (T_{m,hh} + 52)^i + a_3 \Psi^{-1} + \sum_{i=4}^{5} a_i \Psi^{i-2} + \sum_{i=6}^{7} a_i \Psi \, (T_{m,hh} + 52)^{i-4} + a_8 \Psi^2 (T_{m,hh} + 52) \qquad (2)$$

with the a_i's listed in Table 2. Residuals associated with calculation of the total salinity in terms of weight percent (S_{wt}) using Eqn (2) are generally within ± 5 % of experimental values, excluding one outlier (Fig. 3). Equation (2) does not significantly improve on the residuals associated with the equation of NADEN (1996) for the hydrohalite field (Fig. 3); however, the equation of NADEN (1996) tends to over-fit the data, and isotherms generated using NADEN's equation have local extrema between data points, (at some temperatures crossing the H+HH peritectic curve to predict compositions that are within the halite field) (Fig. 4). Isotherms generated using Eqn. (2) are smooth and without local extrema (Fig. 4), and thus better reflect the geometry of the hydrohalite liquidus surface.

Halite field

The liquid salinity on the halite liquidus is described by:

$$\begin{aligned} S_{mol} = & \sum_{i=0}^{3} a_i (T_{m,h} + 52)^i + a_4 \Psi^{-1} + \sum_{i=5}^{6} a_i \Psi \, (T_{m,h} + 52)^{i-3} \\ & + \sum_{i=7}^{9} a_i \Psi^2 (T_{m,h} + 52)^{i-7} + \exp(-T_{m,h} - 52) \end{aligned} \qquad (3)$$

Values of the fitting cofficients a_i are listed in Table 2. Residuals for Eqn. (3) are shown in Figure 3. In addition, the data of ZHANG et al. (1995) along the NaCl-$CaCl_2$ binary are predicted by Eqn. (3) to within ± 4 %, even though the ZHANG et al. data were not included in the regression analysis. In comparison to Eqn. (3), the equation of NADEN (1996) for the halite

liquidus surface predicts wavy isotherms with local extrema, compared to the smooth, monotonic isotherms generated using Eqn. (3) and shown on Fig. 5. The equation of NADEN (1996) also does not adequately reproduce the high salinity H_2O-NaCl binary data of STERNER et al. (1988) (Fig. 3). WILLIAMS-JONES and SAMSON (1990) developed a theoretical equation to calculate halite solubility on the halite liquidus surface, and they report their results graphically as isotherms on the ternary phase diagram. WILLIAMS-JONES and SAMSON (1990) do not provide an error analysis of their model, and their model cannot be compared directly to our results because they do not provide the values for the Pitzer parameters, which they obtained from graphical interpolation. However, based on visual inspection, the isotherms presented by WILLIAMS-JONES and SAMSON (1990) appear to be in good agreement with those predicted by our Eqn. (3).

Antarcticite field

The salinity on the antarcticite liquidus surface is described by the following relationship:

$$S_{mol} = \sum_{i=0}^{5} a_i (T_{m,ant} + 52)^i + \sum_{i=6}^{7} a_i \Psi^{i-5} (T_{m,ant} + 52)^{i-6} \quad (4)$$

Values of the fitting parameters, a_i, are listed in Table 2. Residuals associated with Eqn. (4) are all within ± 5 % of the experimental values (Fig. 3). To our knowledge, no equations have been published previously that describe the relationship between salinity and temperature on the H_2O-NaCl-$CaCl_2$ ternary antarcticite liquidus surface.

Tetrahydrate and dihydrate fields

Quantitative representation of the tetrahydrate and dihydrate fields is limited by the scarcity of available experimental data; however, the narrow compositional range of these fields (Fig. 1c) limits the absolute error in the weight fraction of NaCl in the solution (Φ) to <0.058. The form of each of the equations for the tetrahydrate and dihydrate fields was based in part on

the requirement that the cotectic and peritectic curves bounding these fields must be predicted by the intersection of the equations for the adjacent liquidus fields, because the locations of isotherms in those fields are better constrained than those in the tetrahydrate and dihydrate fields and thus provide a means of checking the validity of the expressions for those fields. The salinity on the tetrahydrate liquidus surface is described by

$$S_{mol} = \sum_{i=0}^{2} a_i (T_{m,Ca4h} + 52)^i + \sum_{i=3}^{4} \Psi \, (T_{m,Ca4h} + 52)^{i-3} + \exp(100\Psi - 10) \quad (5)$$

and the salinity on the dihydrate liquidus surface is described by

$$S_{mol} = \sum_{i=0}^{3} a_i (T_{m,Ca2h} + 52)^i + a_4 \Psi \quad (6)$$

The a_i parameters are listed in Table 2. Residuals of Eqn. (5) are all within ± 2 % of experimental values, and those for Eqn. (6) are within ± 3 %.

Comparison with data for the binary systems

The equations described above for modeling the ternary H_2O-NaCl-$CaCl_2$ system may also be used to predict liquidi for the binary H_2O-NaCl and H_2O-$CaCl_2$ systems using Eqns. (1) to (6), as shown on Figure 6. The predicted H_2O-NaCl eutectic (E') is at -21.18°C, compared to the experimentally determined -21.2°C (HALL et al., 1988). The predicted H_2O-NaCl peritectic point (P') is at +0.14°C, compared to the experimental value of +0.1°C (LINKE, 1958). The predicted H_2O-$CaCl_2$ eutectic point (E") is at -49.9°C, compared to the experimentally determined temperature of -49.8°C (YANATIEVA, 1946). The predicted first and second H_2O-$CaCl_2$ peritectic points (P_1" and P_2") are at +30.0°C and +44.7°C, respectively, compared to the experimental values of +30.1°C and +45.1°C (LINKE, 1958).

Phase Boundary Curves

Each univariant curve is represented by the intersection of the adjacent divariant surfaces, rather than by a separate equation, as discussed above. For example, the liquid composition on the I+HH cotectic is represented by the intersection of the ice and hydrohalite liquidi, or in other words by the collection of T-X conditions that simultaneously satisfy Eqns. (1) and (2). Metastable extensions are not represented in this model. Residuals associated with determining the total salinity in weight percent (S_{wt}) and the weight fraction of NaCl (Φ) along the phase boundary curves by this method are shown in Figures 7 and 8, respectively. Residuals associated with salinity estimation are all within ± 4 % for the I+HH and HH+A cotectics, and within ± 6 % for the HH+H peritectic curve and H+$CaCl_2 \cdot nH_2O$ cotectics (Fig. 7). Percent residuals associated with estimation of Φ on the phase boundary curves are generally larger, with ± 20 % for the I+HH curve, ± 5 % for the HH+A curve, ± 60 % for the HH+H curve, and ± 50 % for the H+ $CaCl_2 \cdot nH_2O$ curves (Fig. 8). These large percent errors in part reflect the fact that Φ is a small number (< 1), such that small absolute errors yield large percent errors. It also reflects some scatter in the experimental data that we intentionally did not attempt to over-fit, owing to our requirement that the phase boundary curves predicted by the equations must be smooth and monotonic.

Identifying pairs of liquidus equations that provided smooth cotectic and peritectic curves that accurately reproduced the experimental values involved some trial and error. In some cases, while the individual equations for the liquidus fields adequately reproduced data in those fields, their intersections sometimes showed significant offset in isotherms on the cotectic or peritectic curves, or did not intersect at experimentally-determined T-X conditions on these curves, or produced topologies for the curves that were not supported by experimental data. As an example,

we found that the equation for the H+HH peritectic curve from NADEN (1996) that describes the weight fraction of NaCl (Φ) as a function of the melting temperature of hydrohalite on the peritectic curve ($T_{pb,hh}$) is over-fitted and predicts an unrealistic curvature, whereas the intersection of Eqns. (2) and (3) from this study is comparably much smoother (Fig. 9). BAKKER (2003) incorporated the equations of OAKES et al. (1990) and NADEN (1996), without modification, into a computer package that added the option to model the univariant curves by the intersections of the adjacent liquidus surfaces (the same approach taken in this study). However, the equations of NADEN (1996) for the hydrohalite and halite liquidi intersect along a wavy curve with local extrema in salinity, which causes anomalous predictions from the computer package of BAKKER (2003), whereas Eqns. (1) and (3) from the present study intersect more smoothly and without extrema (Fig. 10).

Some structure is observable in the residuals associated with the H+$CaCl_2$·nH_2O cotectics and the HH+A cotectic (Figs. 7 and 8). This structure could be reduced or eliminated by adjusting equations for the adjacent fields; however, this approach would then compromise the degree to which those equations for the adjacent fields would reproduce experimental data for those fields. As such, we chose to give preference to achieving the most accurate fit on the I+HH and HH+H boundaries, because phase changes along those boundaries are reported more commonly in studies of natural fluid inclusions. Thus, we have to some extent sacrificed the fidelity with which data along the less commonly reported HH+A and H+$CaCl_2$·nH_2O curves are reproduced. However, we believe that this approach is justified because the antarcticite, tetrahydrate and dihydrate fields encompass a very narrow range of weight fraction NaCl (Φ < 0.05), and the liquid salinity on each of those liquidi surfaces is not very sensitive to the weight

fraction of NaCl. Furthermore, since Φ is always < 0.05 in this part of the system, relatively large percent errors translate into small absolute errors in the weight fraction of NaCl in the inclusion.

Methodologies For Determining Inclusion Bulk Compositions

The model presented here allows fluid inclusion compositions to be determined using a variety of input data, including the melting temperature of a phase on a cotectic or peritectic boundary *and* the temperature of melting of the last solid on the liquidus surface ($T_{pb,x1} + T_{m,x2}$), or the temperature of melting of the last solid on the liquidus surface *and* the weight ratio of NaCl in the inclusion determined from microanalysis ($T_{m,x} + \Phi$), or the melting temperature of two phases on a cotectic or peritectic boundary, either melting simultaneously ($T_{pb,x1} = T_{pb,x2}$) or at different temperatures ($T_{pb,x1} + T_{pb,x2}$). The following sections describe the methodologies to determine bulk composition using the various types of input data.

Final melting on a cotectic curve ($T_{pb,x1} = T_{pb,x2}$, two solid phases dissolve simultaneously)

In the simplest case where two solids dissolve simultaneously on a cotectic curve, the bulk composition is uniquely specified by the melting temperature in accordance with the phase rule. The measured melting temperature can be used to calculate the fluid inclusion composition by solving for the intersection of the adjacent surfaces at that temperature, in other words by finding the value of the weight fraction of NaCl (Φ) for which the two adjacent liquidus surface salinity equations yield the same salinity at the measured temperature of melting. For example, consider a fluid inclusion in which ice and hydrohalite dissolve simultaneously at -25°C. The salinity in the ice field at -25°C and a given weight fraction of NaCl (Φ) can be found from Eqn. (1), while the salinity in the hydrohalite field at -25°C and Ψ can be estimated from Eqn. (2). By iteration, we find that a weight fraction of NaCl, Φ, of 0.57 yields a liquid salinity of 24.7 wt.%

at -25°C in both Eqns. (1) and (2). Thus, the intersection of the ice and hydrohalite liquidus surfaces occurs at a salinity of 24.7 wt.% (NaCl + $CaCl_2$) and a weight fraction of NaCl of 0.57, and this represents the bulk composition of the fluid inclusion.

Last melting temperature ($T_{m,x}$) and NaCl weight fraction (Φ)

If available data include the melting temperature of the last solid obtained from microthermometry, and the weight fraction of NaCl (Φ) determined by microanalysis (e.g., LA-ICPMS), the fluid bulk composition is determined by finding the intersection of the isotherm of the final melting temperature with the pseudobinary defined by the NaCl weight fraction (Φ). Those two variables may be input directly into the appropriate equation (with Φ converted to Ψ where required). As an example, consider a fluid inclusion that contains a halite daughter mineral that dissolves at 200°C, and has a weight fraction of NaCl relative to NaCl + $CaCl_2$ (Φ) of 0.7 based on LA-ICPMS analysis of the inclusion. A weight fraction of NaCl of 0.7 equals a molar fraction, Ψ, of 0.815, and substituting those values of Ψ (0.815) and $T_{m,h}$ (200°C) into Eqn. (3) yields a total salinity on a mole fraction basis, S_{mol}, of 0.116, which corresponds to a total salinity of 33.1 wt.%.

Two unique melting temperatures, $T_{pb,x1}$ + $T_{m,x2}$ or $T_{pb,x1}$ + $T_{pb,x2}$

If available data include two unique melting temperatures from microthermometry – either a cotectic (or peritectic curve) melting temperature ($T_{pb,x1}$) plus the temperature of melting of the last solid phase on the liquidus ($T_{m,x2}$), or a cotectic melting temperature ($T_{pb,,x1}$) plus a univariant peritectic melting temperature ($T_{pb,x2}$) – various calculation procedures may be used depending on which solid phases and phase changes are involved. On Figure 11, the ternary system is divided into several numbered fields that identify compositions within the H_2O-NaCl-

$CaCl_2$ ternary that involve the same phase changes as input data or follow similar calculation procedures.

Field 1 – $T_{pb,hh} < T_{m,ice}$

During heating from the eutectic temperature, fluids with compositions in field 1 (Fig. 11) lose hydrohalite along the I+HH cotectic and ice is the last solid phase to melt on the ice liquidus surface. The composition of the liquid at the temperature of hydrohalite dissolution on the cotectic is determined from the intersection of the hydrohalite and ice liquidi at the temperature of hydrohalite melting ($T_{pb,hh}$), from Eqns. (1) and (2). After hydrohalite disappears, because the last remaining solid is pure H_2O ice (solid solution between solid phases in this system is negligible), the weight fraction of NaCl (Φ) of the liquid phase does not change during continued heating and ice melting, and the liquid composition moves directly towards the H_2O apex. Thus, the weight fraction of NaCl (Φ) determined from the temperature of hydrohalite melting on the cotectic and the final ice melting temperature ($T_{m,ice}$), can be input directly into Eqn. (1) to determine the bulk salinity.

Field 2 – $T_{pb,ant}<T_{m,ice}$

The calculation procedure to determine the composition of fluids that exhibit antarcticite dissolution on the I+A cotectic, followed by final melting of ice on the ice liquidus surface (field 2; Fig. 11) is analogous to that for fluids in field 1, substituting $T_{pb,ant}$ for $T_{pb,hh}$, and substituting Eqn. (4) for Eqn. (2).

Field 3 – $T_{pb,ice}<T_{m,hh}$

For fluid inclusions in which ice is the phase that disappears along the I+HH cotectic and which subsequently show hydrohalite as the last solid to melt on the hydrohalite liquidus (field 3;

Fig. 11), the liquid composition at the temperature of ice melting on the I+HH cotectic is determined from the intersections of Eqns. (1) and (2), as described previously for field 1. After ice melts on the ice-hydrohalite cotectic curve, with further heating the liquid composition evolves along a straight line extending from the composition of the liquid at $T_{pb,ice}$ to the composition of hydrohalite (61.86 wt.% NaCl). The intersection of that line with the isotherm of hydrohalite dissolution yields the unique bulk fluid composition. As an example, consider a fluid inclusion in which ice melts on the I+HH cotectic at -25°C and hydrohalite is the last solid to melt at -10°C. At the last ice melting temperature, the liquid contains 14.3 wt.% NaCl and 10.4 wt.% $CaCl_2$, from the intersection of Eqns. (1) and (2) at $T_{pb,ice}$ = -25°C. The fluid inclusion bulk composition lies on a mixing line between the composition of the liquid on the I+HH cotectic and the composition of hydrohalite. The equation of the mixing line can be determined using the slope and intercept method, where the *x*- and *y*-axes are wt.% NaCl and wt.% $CaCl_2$, respectively, and the input *xy* coordinates are the compositions of liquid (14.3 wt.% NaCl, 10.4 wt.% $CaCl_2$) and hydrohalite (61.9 wt.% NaCl, 0 wt.% $CaCl_2$). The equation of this line (in *xy* coordinates) is also the equation of the vertical plane containing the line (in *xyz* coordinates, where the *z*-axis is temperature), because the linear equation of the mixing line is independent of temperature. Thus, by iteratively solving for the pair of values of wt.% NaCl and wt.% $CaCl_2$ that satisfy both this linear equation and Eqn. (2), we find the bulk composition. In our example, a composition of 16.4 wt.% NaCl and 9.9 wt.% $CaCl_2$ satisfies both equalities, and is thus the bulk fluid composition of the inclusion.

Field 4 $T_{pb,ant}<T_{m,hh}$

For fluid inclusions that exhibit antarcticite melting in the presence of hydrohalite along the HH+A cotectic, followed by hydrohalite final melting (field 4; Fig. 11), the calculation

procedure is analogous to that for field 3, the only difference being that $T_{pb,ant}$ is substituted for $T_{pb,hh}$, and the liquid composition on the HH+A boundary is determined from the intersections of Eqns. (2) and (4).

Field 5 $T_{pb,hh}<T_{m,h}$

Fluid inclusions that have compositions within field 5 (Fig. 11) show halite as the last solid phase to melt, and hydrohalite as the next-to-last solid phase to melt. The calculation procedure for fluid inclusion compositions in this field depends on the input data that are available.

For fluid inclusions in field 5 with compositions to the high-salinity side of the line extending from $CaCl_2 \cdot 6H_2O$ to $NaCl \cdot 2H_2O$ (Figs. 1 and 11) (field 5a), the sub-solidus assemblage is halite+hydrohalite+antarcticite, and first melting occurs at the first peritectic P_1 (Fig. 1). At this temperature (-22.4°C), antarcticite is consumed and the liquid composition subsequently evolves along the HH+H peritectic curve, until hydrohalite is consumed at $T_{pb,hh}$. The liquid composition at $T_{pb,hh}$ is determined from the intersection of Eqns. (2) and (3). The liquid composition on the peritectic curve is recast in terms of the molar proportion of $CaCl_2$ relative to $CaCl_2$+H_2O (Ω) according to:

$$\Psi = \frac{S_{mol} - S_{mol}\Psi_{mol}}{1 - S_{mol}\Psi_{mol}} \qquad (7)$$

Upon departure from the HH+H peritectic curve, the value of Ω of the liquid remains constant with further heating, as the liquid composition evolves along a straight line towards the NaCl apex. The fluid inclusion bulk composition is found as the intersection of the vertical plane containing that line of constant Ω with the isotherm of final halite melting.

For fluid inclusions in field 5 that lie within the ice-hydrohalite-antarcticite triangle (fields 5b and 5c) (Fig. 11), first melting occurs at the eutectic and the liquid composition evolves along either the HH+A or HH+I curve until either ice or antarcticite is consumed, after which the liquid composition evolves across the hydrohalite field along a straight line towards the composition of hydrohalite. Upon intersecting the HH+H peritectic curve, halite nucleates and the liquid composition evolves along the HH+H curve until hydrohalite is consumed. The liquid composition then evolves along a straight line towards the NaCl apex with further heating until halite is completely consumed. For each of the fields 5b and 5c, there are thus three melting temperatures that may be observed and recorded ($T_{pb,ice}$ (or $T_{pb,ant}$) + $T_{pb,hh}$ + $T_{m,h}$), and any pair of these is sufficient to fix the bulk fluid composition. VANKO et al. (1988) describe the methods by which either pair of these data may be used to determine the fluid bulk composition. If the data available are $T_{pb,hh}$ and $T_{m,h}$, the method used to calculate the inclusion composition is the same as outlined above for field 5a. However, as discussed by ROEDDER (1984) and VANKO et al. (1988), the final melting of hydrohalite can be difficult to observe, and hydrohalite may persist metastably for several degrees Celsius above the equilibrium melting temperature. For those reasons, it is sometimes more practical to measure $T_{pb,ice}$ + $T_{m,h}$ (VANKO et al., 1988). In that case, the liquid composition is determined at $T_{pb,ice}$ using Eqns. (1) and (2), and the equation of the straight line that extends from the cotectic liquid composition at $T_{pb,ice}$ to the composition of hydrohalite (as described above for field 3) (Fig. 12). The intersection of the vertical plane containing that line with the isotherm of $T_{m,h}$ on the halite liquidus (Eqn. (3)) represents the bulk fluid composition (VANKO et al., 1988) (Fig. 12). Fluid inclusions with compositions in field 5c are treated in a similar manner to those in field 5b, substituting $T_{pb,ant}$ for $T_{pb,ice}$, and substituting Eqn. (4) for Eqn. (1).

Field 6 $T_{pb,ant,\ Ca4h\ or\ Ca2h} < T_{m,h}$

The calculation method for fluid inclusions that exhibit cotectic melting of one of the three $CaCl_2$ hydrates in the presence of halite, followed by halite dissolution as the last solid phase, is similar for each of the three halite+$CaCl_2 \cdot nH_2O$ cotectics. Field 6a includes fluid inclusion compositions for which antarcticite disappears on the H+A cotectic, field 6b includes those that lose tetrahydrate along the H+Ca4h cotectic, and field 6c includes those that lose dihydrate on the H+Ca2h cotectic (Fig. 11). The method employed for each of these fields is to determine the liquid composition (Ω) on the cotectic at the temperature of last hydrate melting from the intersection of Eqn (3) with either Eqn. (4), Eqn. (5) or Eqn. (6) (depending on the last hydrate to melt). The fluid inclusion bulk composition is found as the intersection of the vertical plane containing the line of constant Ω with the isotherm of final halite melting ($T_{m,h}$).

Field 7 – $T_{pb,x} < T_{m,ant,\ Ca4h\ or\ Ca2h}$

Field 7 (Fig. 11) includes a narrow compositional range near the $CaCl_2$ binary, and is characterized by at least seven possible melting sequences and pairs of input data, although observation of melting sequences in this part of the system has yet to be reported unequivocally for natural fluid inclusions.

Because the weight fraction of NaCl (Φ) in this part of the system is everywhere less than 0.05, the fluid bulk composition can be estimated with reasonable precision from $T_{m,CaCl2 \cdot nH2O}$ alone. The liquid Φ on the appropriate cotectic or peritectic curve can be determined directly as outlined for the other fields, by the intersection of the adjacent liquidi, and the bulk composition lies on the straight line that extends from that composition to the composition of the final melting of solid $CaCl_2$ hydrate. Again, the weight fraction of NaCl (Φ) in the bulk fluid in this part of the

system does not significantly affect the calculated total salinity and, in the absence of a next-to-last melting temperature, Φ must be between 0-0.05.

Description of the Numerical Model

The numerical model developed in this study has been built into a Microsoft® Excel© program that estimates H_2O-NaCl-$CaCl_2$ fluid inclusion compositions. The program is available for download as an electronic annex to this paper. Compositions that may be calculated using the model are defined by a triangle bounded by the H_2O apex, the NaCl apex and the composition of $CaCl_2 \cdot 4H_2O$ on the H_2O-$CaCl_2$ binary (Fig. 13). For comparison, the compositional limits of other published numerical models (CalcicBrine (NADEN, 1996); Aqso1e and AqSo2e (BAKKER, 2003); "H2O_NaCl-CaCl2" (CHI and NI, 2007)) are also shown in Figure 13. The compositional range of the numerical model developed in this study extends the applicability to fluid inclusions that have liquid compositions that evolve along an antarcticite-bearing cotectic curve, as well as fluid inclusions that exhibit first melting at the first or second ternary peritectic, for which the composition cannot be determined using the previously published models. The programs "H2O_NaCl_CaCl2" (CHI and NI, 2007) and "AqSo2e" (BAKKER, 2003) do not allow the input of a known weight fraction of NaCl (Φ) to calculate fluid inclusion bulk composition. Furthermore, "AqSo2e" (BAKKER, 2003) does not allow the input of the combination of melting of ice on a cotectic or peritectic ($T_{pb,ice}$) *and* melting of halite on the liquidus surface ($T_{m,h}$).

Examples of Application of the Model to Natural Fluid Inclusions

Application of the numerical model developed in this study to interpretation of natural fluid inclusions can be demonstrated using data from previously published studies. Where

available, data for individual fluid inclusions have been input into the numerical model derived in this study to determine bulk fluid compositions. In other cases, ranges of measured temperatures of phase transitions have been input into the model to estimate ranges in fluid compositions.

Fluid inclusions that show ice as the final solid phase to melt are reported in many studies (e.g., see BASUKI and SPOONER (2002) for references). The "Stage III" inclusions in epidote of LAYNE and SPOONER (1991) are used as examples here to demonstrate the applicability of the numerical model developed in the present study. The compositions of these fluid inclusions, determined using the microthermometric data of LAYNE and SPOONER (1991) in the numerical model developed in this study range from 17.4 to 26.5 wt.% total salt, and a weight fraction of NaCl (Φ) of 0.064 to 0.081 (Fig. 14). These compositions are in good agreement with those reported by LAYNE and SPOONER (1991), differing by less than 1 wt.% total salinity for each inclusion (Table 3).

Fluid inclusions in which hydrohalite is the last solid to melt have been reported by, among others, NYMAN et al. (1990), LAYNE and SPOONER (1991), and XU (2000). The microthermometric data of NYMAN et al. (1990) are reported only as temperature ranges, and the minimum and maximum melting temperatures were used to estimate the range of fluid inclusion compositions using our numerical model (Fig. 14; Table 3). The range in salinities determined here based on the microthermometric data of NYMAN et al. (1990) is 26.4 to 30.4 wt. % NaCl, with a range in weight fraction of NaCl (Φ) of 0.16 to 0.63, whereas NYMAN et al. (1990) report salinities of 26 to 27 wt.% NaCl and Φ from 0.6 to 0.7. The difference in Φ reported by NYMAN et al. (1990) compared to values determined in this study is likely due to the inaccuracy associated with graphically interpolating isotherms in the hydrohalite field that was used in the

previous study, compared to the numerical methods used here. However, the bulk salinities estimated by NYMAN et al. (1990) are in good agreement with those estimated here.

Natural fluid inclusions that show halite as the final solid to melt are described by VANKO et al. (1988), NYMAN et al. (1990), SCHIFFRIES (1990), LAYNE and SPOONER (1991) and XU (2000). Microthermometric data from VANKO et al. (1988) for individual fluid inclusions in quartz from a vein in hornblendite from the Mathematician Ridge, East Pacific Rise, have been used to estimate fluid inclusion compositions (Fig. 14). Those fluid inclusions from VANKO et al. (1988) in which ice melts in the presence of metastable halite have been excluded in this example. The compositions of the fluid inclusions determined using our numerical model are in good agreement with the compositions determined by VANKO et al. (1988), differing by less than 2 wt.% for each inclusion (Table 3).

Microthermometric data from "Type 1" and "Type 3" inclusions from the Bushveld Complex reported by SCHIFFRIES (1990) include cotectic melting temperatures of various $CaCl_2$ hydrates. SCHIFFRIES (1990) did not estimate a bulk fluid composition due the uncertainty in locating the H+A and H+Ca2h cotectic curves, and the small number of experimental data in this part of the phase diagram (SCHIFFRIES, 1990). The "Type 1" inclusions exhibit eutectic melting, and the liquid evolves along the H+A cotectic before losing antarcticite ($T_{pb,ant}$) and undergoing final melting by halite dissolution ($T_{m,h}$). The data for "Type 1" inclusions indicate salinities ranging from 46 to 51 wt.% total salt and weight fraction of NaCl (Φ) ranging from 0.15 to 0.24 (Fig. 14; Table 3). The "Type 3" inclusions of SCHIFFRIES (1990) show first melting at the second ternary peritectic (P_2) (Fig. 1), and the liquid evolves along the H+Ca4h cotectic before losing tetrahydrate ($T_{pb,Ca4h}$), and the last solid phase to melt is halite ($T_{m,h}$). The ranges of

613 $T_{pb,Ca4h}$ and $T_{m,h}$ from SCHIFFRIES (1990) indicate salinities for the "Type 3" inclusions of 49 to
614 54 wt.% total salt, with Φ ranging from 0.14 to 0.25 (Fig. 14; Table 3).

615 No examples are given in Figure 14 and Table 3 of fluid inclusions in which antarcticite
616 is the last solid phase to melt, because fluid inclusions of this type have not been unequivocally
617 identified in previous studies. The apparent lack of fluid inclusions of this type may be due in
618 part to the narrow compositional range of the antarcticite field (Fig. 1), but also possibly due to
619 the difficulty of recognizing antarcticite in fluid inclusions (see ROEDDER, 1984). For example,
620 ROBERT and KELLEY (1987) identified salt hydrate as the last melting phase of some H_2O-NaCl-
621 $CaCl_2$ fluid inclusions from gold-bearing quartz veins at the Sigma Mine, but were unable to
622 determine whether the phase was hydrohalite or antarcticite. ULMER-SCHOLLE et al. (1993)
623 report antarcticite as the final solid phase to melt in fluid inclusions in diagenetic quartz from the
624 Delaware Basin (Texas and New Mexico), but the identification was based on melting
625 temperatures up to +3.1°C for fluid inclusions with homogenization temperatures of 53-81°C
626 (ULMER-SCHOLLE et al., 1993). Fluid inclusions with such low homogenization temperatures
627 tend to eliminate the vapor bubble upon freezing, due to the volume expansion associated with
628 the water-ice transition, and thus the melting temperatures were obtained under vapor-absent
629 conditions. Under such conditions, the temperatures of solid-liquid phase transitions cannot be
630 properly interpreted with respect to experimental data for the vapor-saturated liquidus
631 (ROEDDER, 1967). As shown by ROEDDER (1967), a final melting temperature of +3.1°C is not
632 incompatible with metastable melting of ice in the pure H_2O system under vapor-absent
633 conditions.

634 Although fluid inclusions that have antarcticite as the final solid phase to melt have not
635 been unambiguously identified, fluid inclusions with low NaCl weight fraction (Φ) (e.g., KWAK

and TAN, 1981; LAYNE and SPOONER, 1991) as well as those described by SCHIFFRIES (1990) in which the liquid composition evolves along the H+A and H+Ca4h cotectics, indicate that fluid compositions in the $CaCl_2$-rich portion of the phase diagram occur in nature. Furthermore, Raman analysis has been used to identify $CaCl_2$ hydrates in fluid inclusions (DUBESSY et al., 1982; SAMSON and WALKER, 2000; BAUMGARTNER and BAKKER, 2009). The numerical model developed in this study allows fluid compositions to be determined in this part of the phase diagram, and will be useful if fluid inclusions with high salinity and low weight fraction of NaCl (Φ) are discovered in the future.

Summary

The empirical equations developed in this study completely describe the geometry of the liquidus surface and cotectic curves for the part of the H_2O-NaCl-$CaCl_2$ phase diagram between the H_2O apex, the NaCl apex and the composition of $CaCl_2 \cdot 4H_2O$ on the H_2O-$CaCl_2$ binary. The numerical model described herein incorporates this comprehensive set of equations to allow fluid inclusion compositions to be determined anywhere within that compositional range, using a variety of combinations of input data. The model has been applied to estimate compositions of natural fluid inclusions using microthermometric data reported in the literature. The Microsoft® Excel© program that implements the model to estimate fluid inclusion compositions is available for download as an electronic annex to this paper. The authors recommend that the model presented here should be used in preference to CalcicBrine.

Acknowledgements

The authors thank Dave Vanko, Iain M. Samson and an anonymous reviewer for their comments and suggestions that significantly clarified, improved and shortened an earlier version of this manuscript. The authors also thank Associate Editor Bob Burruss for his comments and sage advice on editorial issues. Thanks to Tobias Schlegel for testing the computer package and suggesting some improvements to the user interface. This material is based upon work supported by the National Science Foundation under grant nos. EAR-0711333 and OCE-0928472. The Institute for Critical Technology and Applied Science (ICTAS) at Virginia Tech provided support for Steele-MacInnis. Naden publishes with the permission of the Executive Director, British Geological Survey (NERC).

668 **References**

669 Bakker, R. J., 2003. Package FLUIDS; 1, Computer programs for analysis of fluid inclusion data
670 and for modelling bulk fluid properties. *Chemical Geology* **194**, 3-23.
671 Basuki, N. I. and Spooner, E. T. C., 2002. A review of fluid inclusion temperatures and salinities
672 in Mississippi valley-type Zn-Pb deposits; identifying thresholds for metal transport.
673 *Exploration and Mining Geology* **11**, 1-17.
674 Baumgartner, M. and Bakker, R. J., 2009. $CaCl_2$-hydrate nucleation in synthetic fluid inclusions.
675 *Chemical Geology* **265**, 335-344.
676 Bodnar, R. J., 1994. Synthetic fluid inclusions; XII, The system H_2O-NaCl; experimental
677 determination of the halite liquidus and isochores for a 40 wt% NaCl solution.
678 *Geochimica et Cosmochimica Acta* **58**, 1053-1063.
679 Chi, G. and Ni, P., 2007. Equations for calculation of NaCl/(NaCl + $CaCl_2$) ratios and salinities
680 from hydrohalite-melting and ice-melting temperatures in H_2O-NaCl-$CaCl_2$ system.
681 *Yanshi Xuebao* **23**, 33-37.
682 Chou, I-Ming, 1987. Phase relations in the system NaCl-KCI-H_2O. Part III: Solubilities of halite
683 in vapor-saturated liquids above 445°C and redetermination of phase equilibrium
684 properties in the system NaCl-$H_2$0 to 1000°C and 1500 bars. *Geochimica et*
685 *Cosmochimica Acta **51**, 1965-1975.*
686 Collins, A. G., 1975. *Geochemistry of oilfield waters*. Elsevier Scientific Publishing Company,
687 Amsterdam; New York.
688 Dubessy, J., Audeoud, D., Wilkins, R., and Kosztolanyi, C., 1982. The use of the Raman
689 microprobe MOLE in the determination of the electrolytes dissolved in the aqueous phase
690 of fluid inclusions. *Chemical Geology* **37**, 137-150.

691 Frape, S. K., Fritz, P., and McNutt, R. H., 1984. Water-rock interaction and chemistry of
692 groundwaters from the Canadian Shield. *Geochimica et Cosmochimica Acta* **48**, 1617-
693 1627.
694 Günther, D., Audetat, A., Frischknecht, R., and Heinrich, C. A., 1998, Quantitative analysis of
695 major, minor and trace elements in fluid inclusions using laser ablation - inductively
696 coupled plasma mass spectrometry: Journal of Analytical Atomic Spectroscopy, **13**, p.
697 263-270.
698 Hall, D.L., Sterner, S.M. and Bodnar, R.J., 1988, Freezing point depression of NaCl-KCl-H_2O
699 solutions. *Economic Geology and the Bulletin of the Society of Economic Geologists*, **83**,
700 197-202.
701 Hanor, J. S. and McIntosh, J. C., 2007. Diverse origins and timing of formation of basinal brines
702 in the Gulf of Mexico sedimentary basin. *Geofluids* **7**, 227-237.
703 Haynes, F. M. and Kesler, S. E., 1987. Chemical evolution of brines during Mississippi valley-
704 type mineralization; evidence from East Tennessee and Pine Point. *Economic Geology*
705 *and the Bulletin of the Society of Economic Geologists* **82**, 53-71.
706 Konnerup-Madsen, J., 1979. Fluid inclusions in quartz from deep-seated granitic intrusions,
707 south Norway. *Lithos* **12**, 13-23.
708 Kwak, T. A. P. and Tan, T. H., 1981. The importance of $CaCl_2$ in fluid composition trends;
709 evidence from the King Island (Dolphin) skarn deposit. *Economic Geology and the*
710 *Bulletin of the Society of Economic Geologists* **76**, 955-960.
711 Layne, G. D. and Spooner, E. T. C., 1991. The JC tin skarn deposit, southern Yukon Territory; I,
712 Geology, paragenesis, and fluid inclusion microthermometry. *Economic Geology and the*
713 *Bulletin of the Society of Economic Geologists* **86**, 29-47.

Li, C. and Naldrett, A. J., 1993. High chlorine alteration minerals and calcium-rich brines in fluid inclusions from the Strathcona deep copper zone, Sudbury, Ontario. *Economic Geology and the Bulletin of the Society of Economic Geologists* **88**, 1780-1796.

Linke, W. F., 1958. *Solubilities, inorganic and metal organic compounds; a compilation of solubility data from the periodical literature*. Van Nostrand, Princeton, NJ.

Lowenstein, T. K., Hardie, L. A., Timofeeff, M. N., and Demicco, R. V., 2003. Secular variation in seawater chemistry and the origin of calcium chloride basinal brines. *Geology* **31**, 857-860.

Naden, J., 1996. CalcicBrine; a Microsoft Excel 5.0 add-in for calculating salinities from microthermometric data in the system NaCl-$CaCl_2$-H_2O. In: Brown, P. E. and Hagemann, S. G. Eds.)*PACROFI VI*, Madison, WI.

National Research Council, 1928. *International critical tables of numerical data, physics, chemistry and technology*. McGraw-Hill, New York.

Nyman, M. W., Sheets, R. W., and Bodnar, R. J., 1990. Fluid-inclusion evidence for the physical and chemical conditions associated with intermediate-temperature PGE mineralization at the New Rambler Deposit, southeastern Wyoming. *The Canadian Mineralogist* **28**, 629-638.

Oakes, C. S., Bodnar, R. J., and Simonson, J. M., 1990. The system NaCl-$CaCl_2$-H_2O; 1, The ice liquidus at 1 atm total pressure. *Geochimica et Cosmochimica Acta* **54**, 603-610.

Oakes, C. S., Sheets, R. W., and Bodnar, R. J., 1992. (NaCl + $CaCl_2$)[aq]; phase equilibria and volumetric properties. In: Hall, D. S. and Sterner, S. M. Eds.)*PACROFI IV Extended Abstracts*, Lake Arrowhead, CA.

Potter, R. W., II and Clynne, M. A., 1978. Solubility of highly soluble salts in aqueous media; Part 1, NaCl, KCl, $CaCl_2$, Na_2SO_4 , and K_2SO_4 solubilities to 100°C. *Journal of Research of the U. S. Geological Survey* **6**, 701-705.

Robert, F. and Kelly, W. C., 1987. Ore-forming fluids in Archean gold-bearing quartz veins at the Sigma Mine, Abitibi greenstone belt, Quebec, Canada. *Economic Geology and the Bulletin of the Society of Economic Geologists* **82**, 1464-1482.

Roedder, E., 1967. Metastable superheated ice in liquid water inclusions under high negative pressure. *Science* **155**, 1412-1417.

Roedder, E., 1984. Fluid inclusions. *Reviews in Mineralogy* **12**, 644.

Samson, I. M. and Walker, R. T., 2000. Cryogenic Raman spectroscopic studies in the system NaCl-$CaCl_2$-H_2O and implications for low-temperature phase behavior in aqueous fluid inclusions. *The Canadian Mineralogist* **38**, 35-43.

Samson, I. M., Williams-Jones, A. E., Ault, K. M., Gagnon, J. E. & Fryer, B. J. (2008). Source of fluids forming distal Zn-Pb-Ag skarns: Evidence from laser ablation-inductively coupled plasma-mass spectrometry analysis of fluid inclusions from El Mochito, Honduras. *Geology* **36**, 947-950.

Schiffries, C. M., 1990. Liquid-absent aqueous fluid inclusions and phase equilibria in the system $CaCl_2$-NaCl-H_2O. *Geochimica et Cosmochimica Acta* **54**, 611-619.

Sterner, S. M., Hall, D. L., and Bodnar, R. J., 1988. Synthetic fluid inclusions. V. Solubility relations in the system NaCl-KCl-H_2O under vapor-saturated conditions. *Geochimica et Cosmochimica Acta* **52**, 989-1005.

Stoffell, B., Appold, M. S., Wilkinson, J. J., McClean, N. A. & Jeffries, T. E. (2008). Geochemistry and evolution of Mississippi valley-type mineralizing brines from the Tri-

State and Northern Arkansas Districts determined by LA-ICP-MS microanalysis of fluid inclusions. *Economic Geology and the Bulletin of the Society of Economic Geologists* **103**, 1411-1435.

Ulmer-Scholle, D. S., Scholle, P. A., and Brady, P. V., 1993. Silicification of evaporites in Permian (Guadalupian) back-reef carbonates of the Delaware Basin, West Texas and New Mexico. *Journal of Sedimentary Petrology* **63**, 955-965.

Vanko, D. A., 1988. Temperature, pressure, and composition of hydrothermal fluids, with their bearing on the magnitude of tectonic uplift at mid-ocean ridges, inferred from fluid inclusions in oceanic layer 3. *Journal of Geophysical Research* **93**, 4595-4611.

Vanko, D. A., Bodnar, R. J., and Sterner, S. M., 1988. Synthetic fluid inclusions; VIII, Vapor-saturated halite solubility in part of the system NaCl-$CaCl_2$-H_2O, with application to fluid inclusions from oceanic hydrothermal systems. *Geochimica et Cosmochimica Acta* **52**, 2451-2456.

Williams-Jones, A. E. and Samson, I. M., 1990. Theoretical estimation of halite solubility in the system NaCl-$CaCl_2$-H_2O; applications to fluid inclusions. *The Canadian Mineralogist* **28**, 299-304.

Xu, G., 2000. Fluid inclusions with NaCl-$CaCl_2$-H_2O composition from the Cloncurry hydrothermal system, NW Queensland, Australia. *Lithos* **53**, 21-35.

Yanatieva, O. K., 1946. Solubility polytherms in the systems $CaCl_2$-$MgCl_2$-H_2O and $CaCl_2$-NaCl-H_2O. *Zhurnal Prikladnoi Khimii* **19**, 709-22.

Zhang, Y., Han, Y., and Wang, S, 1995. Phase diagram of the ternary system $SmCl_3$-NaCl-$CaCl_2$. *Thermochimica Acta* **254**, 383-90.

Appendix A. Stable Melting Paths of H_2O-NaCl-$CaCl_2$ Fluid Inclusions

The compositions of natural fluid inclusions that are described by the system H_2O-NaCl-$CaCl_2$ may be determined based on the temperature and sequence of phase changes observed during heating from low temperatures. The temperatures of phase changes and the sequence of phase changes, in turn, depend on the bulk composition of the inclusion. The temperature of first melting provides an indication of which representative system is appropriate for interpreting the fluid inclusion composition, and may also provide an indication of the compositional range (e.g., first melting at the eutectic versus first melting at a peritectic point). However, the phase changes that are most often used to determine bulk compositions of fluid inclusions from microthermometric data are the melting temperatures of the last and next-to-last solid phases, so it is not necessary to measure the temperatures of all phase changes. The reader is referred to SCHIFFRIES (1990) for a complete discussion of the many potential stable melting pathways in the H_2O-NaCl-$CaCl_2$ system, and to VANKO et al. (1988) and BAUMGARTNER and BAKKER (2009) for some examples of metastable melting sequences. Note that if the last or next-to-last solid phase to melt is metastable, it can lead to misinterpretation of the fluid inclusion composition, as discussed by ROEDDER (1984) and BAUMGARTNER and BAKKER (2009).

Fluid inclusions approximated by the system H_2O-NaCl-$CaCl_2$ and having compositions that lie within the ice-hydrohalite-antarcticite triangle (triangle "1"; Fig. 1b) are characterized by the subsolidus assemblage ice+hydrohalite+antarcticite, and have first melting at the ternary eutectic (E) at -52°C (Fig. 1c). The vapor bubble (the presence of which is required to demonstrate vapor-saturated conditions) is considered to be of

805 negligible mass and does not contribute to the fluid composition (except perhaps for high
806 temperature (≥ 400°C) fluid inclusions that contain a vapor bubble larger than a few 10's
807 of volume percent at the time of last melting). Inclusions with compositions that lie
808 within the hydrohalite+halite+antarcticite triangle (triangle "2"; Fig. 1b) contain the
809 subsolidus assemblage hydrohalite+halite+antarcticite. For these compositions, first
810 melting occurs at the first peritectic point (point "P_1"; Fig. 1c), and the first solid phase to
811 be consumed is antarcticite. SCHIFFRIES (1990) has also identified fluid inclusions that are
812 liquid-absent at room temperature and characterized by the sub-solidus assemblage
813 antarcticite+halite+tetrahydrate (triangle "3"; Fig. 1b) and exhibit first melting at the
814 second ternary peritectic (P_2) (Fig. 1c) at +29°C (SCHIFFRIES, 1990). Fluid inclusions
815 showing second peritectic (or higher) first melting behavior are liquid-absent at room
816 temperature and can be easily overlooked or mistaken for mineral inclusions during
817 routine petrographic examination (SCHIFFRIES, 1990).

818 Natural H_2O-NaCl-$CaCl_2$ fluid inclusions that show ice as the last solid phase to
819 melt have been described in many studies and are common in MVT deposits (e.g., see
820 BASUKI and SPOONER, 2002). For inclusions that have ice as the last solid phase to melt
821 the liquid composition may evolve along either the I+HH cotectic (path E→a1; Fig. A1-
822 a) or the I+A cotectic (path E→a3; Fig. A1-a) during heating from the eutectic
823 temperature, depending on the bulk composition. Thus, the melting temperature of ice
824 ($T_{m,ice}$) will be preceded by melting of hydrohalite ($T_{pb,hh}$) (path E→a1→a2, Fig. A1-a)
825 for inclusions that contain more than 0.058 weight fraction of NaCl (Φ) relative to NaCl
826 + $CaCl_2$, corresponding to the composition at the eutectic, but the melting temperature of

ice will be preceded by $T_{pb,ant}$ (path E→a3→a4, Fig. A1-a) if the bulk composition lies to the $CaCl_2$-rich side of the eutectic composition ($\Phi = 0.058$).

For fluid inclusions whose bulk composition lies within the hydrohalite field, hydrohalite is the last solid phase to melt and either ice or antarcticite must be the next-to-last solid phase to melt. Thus, the melting temperature of hydrohalite ($T_{m,hh}$) is preceded by either the melting of ice ($T_{pb,ice}$; path E→b1→b2; Fig. A1-b) or the melting of antarcticite ($T_{pb,ant}$; path E→b3→b4; Fig. A1-b). The fluid composition evolves directly toward the composition of hydrohalite upon departure from the I+HH or HH+A cotectic (path segments b1→b2 and b3→b4, respectively; Fig. A1-b), until final melting occurs by hydrohalite disappearance (points "b2" and "b4"; Fig. A1-b). Natural fluid inclusions that show hydrohalite as the last solid to melt have been described by NYMAN et al. (1990), LAYNE and SPOONER (1991) and XU (2000).

Fluid inclusions with bulk compositions in the halite field may lose ice on the I+HH cotectic (path E→c1→c2 →c3→c4; Fig. A1-c) or lose antarcticite on the HH+A cotectic (path E→c5→c6 →c7→c8 ; Fig. A1-c). For example, consider a fluid inclusion with bulk composition shown by point "c4" in Figure A1-c. First melting occurs at the eutectic (point "E," Fig. A1-c), where antarcticite is completely consumed. The liquid composition then evolves along the I+HH cotectic upon further heating until ice is completely consumed at point "c1" (Fig. A1-c). Then, the liquid composition evolves across the hydrohalite field along a straight line toward the composition of hydrohalite on the H_2O-NaCl binary. Upon intersection of the HH+H reaction curve at point "c2" hydrohalite reacts to produce halite + liquid. The liquid composition then evolves along the HH+H peritectic curve as halite grows at the expense of hydrohalite, until all

hydrohalite is consumed at point "c3", and the liquid composition then evolves along a straight line towards halite with further heating, until final melting of halite at point "c4", representing the fluid inclusion bulk composition (Fig. A1-c). This melting sequence can theoretically yield temperatures for the melting of ice along the I+HH cotectic ($T_{pb,ice}$) (point "c1"; Fig. A1-c) (or melting of antarcticite along the HH+A cotectic, ($T_{pb,ant}$) (point "c5")), the melting of hydrohalite along the HH+H peritectic ($T_{pb,hh}$) and the melting of halite on the vapor-saturated halite liquidus ($T_{m,h}$) (Fig. 2c). However, in practice the disappearance of the first phase to melt, either ice or antarcticite, may be difficult to recognize, or the melting temperature of hydrohalite may be difficult to determine accurately owing to sluggish melting or metastability, for instance due to the kinetic barrier to halite nucleation on the HH+H peritectic curve. Fluid inclusions that follow this melting sequence have been described in natural samples by VANKO et al. (1988), NYMAN et al. (1990), LAYNE and SPOONER (1991) and XU (2000).

Fluid inclusions with compositions in the halite field can also exhibit liquid evolution along one or more of the halite-$CaCl_2$ hydrate cotectics. For example, consider a fluid inclusion with a bulk composition shown by point "c10" in Figure A1-c. This bulk composition lies within the hydrohalite+halite+antarcticite triangle (triangle "2"; Fig. 1b), so the subsolidus assemblage is hydrohalite+halite+antarcticite. For this composition, first melting occurs at the first peritectic point (point "P_1"; Fig. A1-c), and the first solid phase to be consumed is antarcticite. The liquid composition then evolves along the H+A cotectic until it intersects the second peritectic point (point "P_2"; Fig. A1-c), at which point antarcticite reacts to produce tetrahydrate + liquid. Once antarcticite is completely consumed, the liquid composition evolves along the H+Ca4h cotectic with further

873 heating, until tetrahydrate is completely consumed at point "c9" (Fig. A1-c), after which
874 the liquid composition evolves along a straight line toward the composition of halite
875 (NaCl) until halite is completely consumed at point "c10", representing the fluid
876 inclusion bulk composition. In theory, this melting sequence can provide values for $T_{pb,ant}$
877 (the second peritectic temperature) and $T_{pb,Ca4h}$ along with $T_{m,h}$. Natural fluid inclusions
878 exhibiting this sequence of phase changes have been described by SCHIFFRIES (1990).
879 As pointed out by SCHIFFRIES (1990), several phase change sequences corresponding to
880 compositions within the expected range of geologic fluid compositions have yet to be
881 reported in natural H_2O-NaCl-$CaCl_2$ fluid inclusions. Most notably, natural fluid
882 inclusions in which the last solid phase to melt is a $CaCl_2$ hydrate have yet to be
883 unequivocally identified, although some previous studies have reported a salt hydrate,
884 thought to be antarcticite, as the last solid phase to melt (e.g., ULMER-SCHOLLE et al.,
885 1993), and final melting of $CaCl_2$ hydrates has been observed in synthetic H_2O-$CaCl_2$
886 fluid inclusions (BAUMGARTNER and BAKKER, 2009). Several possible sequences of
887 phase changes are contained within the compositional range of the $CaCl_2$ hydrate liquidi
888 (e.g., paths E→d1→d2 and E→d3→d4; Fig. A1-d).
889

Figure Captions

Figure 1. Vapor-saturated liquidus phase relations in the H_2O-NaCl-$CaCl_2$ system. *(a)* A distorted, schematic representation of the ternary H_2O-NaCl-$CaCl_2$ system showing the relative locations of the liquidus fields. *(b)* The shaded region on the ternary diagram shows the part of the system that is modeled in this study. The numbered triangles show fields of sub-solidus phase assemblages. Bulk compositions within triangle "1" contain the equilibrium assemblage ice+hydrohalite+antarcticite when frozen; those in triangle "2" contain hydrohalite+halite+antarcticite when frozen; and those compositions in triangle "3" contain halite+antarcticite+tetrahydrate when frozen. *(c)* Phase boundaries (cotectic and peritectic curves) and isotherms calculated using the equations developed in this study (see text for discussion). The invariant points and univariant curves are labeled according to the terminology described in the text. Arrows on the univariant curves point up-temperature.

Figure 2. Summary of sources of experimental data for the H_2O-NaCl-$CaCl_2$ system used in this study. The data are sorted according to the phase assemblage on the vapor-saturated liquidus, and the source of the data (see the legend). The phase boundary curves were calculated from the equations derived in this study (described in detail in the text).

Figure 3. Residuals, in percent difference between experimental and calculated values {(1 - calculated/measured)*100%}, associated with the liquid salinity on the vapor-saturated liquidi of ice *(a)*, hydrohalite *(b)*, halite *(c)* and antarcticite *(d)* as a function of the experimental salinity. Calculated salinities are based on the melting temperature of the last solid on the liquidus ($T_{m,x}$) and the weight ratio of NaCl relative to NaCl + $CaCl_2$ (Φ) calculated from Eqns. (1) to (4). The symbols used for the residuals correspond to the equation used and the source of experimental values to which the predicted values are compared (see the legend).

Figure 4. Comparison of the composition (salinity vs. NaCl weight ratio) on the -10°C isotherm on the vapor-saturated hydrohalite liquidus predicted by the equation of NADEN (1996) (dashed line) and by equation (2) from this study (solid line). Experimental data on the -10°C isotherm from YANATIEVA (1946) are shown as open circles.

Figure 5. Comparison of the salinity on the +94.5°C isotherm on the vapor-saturated halite liquidus predicted by the equation of NADEN (1996) (dashed line) and by equation (3) from this study (solid line). Experimental data on the +94.5°C isotherm from the NATIONAL RESEARCH COUNCIL (1928) are shown as open circles. These experimental data were chosen for comparison because of the large number of data points extending over a wide range of compositions along the +94.5°C isotherm in the NRC report.

Figure 6. Liquidus curves for the H_2O-NaCl *(top)* and H_2O-$CaCl_2$ *(bottom)* binary systems, calculated from Eqns. (1) to (6). Experimental data are from NATIONAL RESEARCH COUNCIL (1928) (halite); YANATIEVA (1946) (ice, hydrohalite, halite, antarcticite); LINKE (1958) (ice, hydrohalite, halite, antarcticite, tetrahydrate, dihydrate); POTTER and CLYNNE (1978) (halite, antarcticite, tetrahydrate, dihydrate); STERNER et al. (1988) (halite); and OAKES et al. (1990) (ice).

Figure 7. Residuals, in percent difference between experimental and calculated values {(1 - calculated/measured)*100%}, associated with liquid salinity on the I+HH, HH+H, HH+A and H+$CaCl_2 \cdot n H_2O$ phase boundary curves as a function of temperature from Eqns. (1), (2), (3), (4) and (6), plotted against the experimental salinity. Symbols used are the same as for Figure 3.

Figure 8. Residuals, in percent difference between experimental and calculated values {(1 - calculated/measured)*100%}, associated with Φ on the I+HH, HH+H, HH+A and H+$CaCl_2 \cdot n H_2O$ phase boundary curves as a function of temperature from Eqns. (1), (2), (3), (4) and (6), plotted against the experimental weight fraction of NaCl (Φ). The dashed vertical line in the I+HH residuals plot (upper left) shows the eutectic composition. Symbols used are the same as for Figure 3.

Figure 9. Comparison of the weight fraction of NaCl in the liquid (Φ) as a function of temperature on the HH+H peritectic curve predicted by the equation of NADEN (1996) (dashed line) and by the intersection of equations (2) and (3) from this study (solid line). Experimental data (solid triangles) are from YANATIEVA (1946) and LINKE (1958).

Figure 10. Comparison of the liquid salinity as a function of temperature on the HH+H peritectic curve predicted by the method of intersection of adjacent liquidus surfaces from NADEN (1996), implemented by BAKKER (2003) (dashed line) and by the Equations (1) and (3) from this study (solid line). Experimental data (solid triangles) are from YANATIEVA (1946) and LINKE (1958).

Figure 11. Phase relations in the H_2O-NaCl-$CaCl_2$ system under vapor-saturated conditions showing the eleven different composition fields, based on the sequence and temperatures of the final two (or three) solids to melt during heating. See text for discussion of phase changes corresponding to each field and identification of symbols.

Figure 12. Schematic heating sequence for a fluid inclusion with a composition within field 5b (Fig. 11), showing the melting events that may be observed during microthermometry. Isotherms of the relevant phase changes are shown as dotted lines. Antarcticite is lost at the eutectic (point “E”), . The liquid composition then evolves along the I+HH cotectic with further heating until

ice is consumed at point "a" ($T_{pb,ice}$). At this point, because hydrohalite is the only solid phase present, the liquid composition evolves along a straight line towards the composition of hydrohalite with further heating (segment a→b). The HH+H curve is intersected at point "b," where halite nucleates ($T_{pb,hh*}$). On further heating, the liquid composition evolves along the HH+H peritectic curve (segment b→c), until hydrohalite is consumed at point "c" ($T_{pb,hh}$). At this point, halite is the only remaining solid phase, so with further heating the liquid composition evolves towards the NaCl apex until intersecting the $T_{m,h}$ isotherm at point "d," which is the bulk fluid inclusion composition. Note that the bulk composition lies along the mixing line "a-NaCl·$2H_2O$" (between the liquid composition at $T_{pb,ice}$ and pure hydrohalite), and the mixing line "c-NaCl" (between the liquid composition at $T_{pb,hh}$ and pure halite), therefore any pair of $T_{pb,ice}$, $T_{pb,hh}$ or $T_{m,h}$, is sufficient to fix the bulk composition.

Figure 13. Comparison of the compositional ranges over which the model presented in this study (*top*) and previously published models of the H_2O-NaCl-$CaCl_2$ system are valid (*middle and bottom*). *Top:* The compositional range of applicability of the model presented in this study. *Middle:* The shaded field shows the range of applicability of the model AqSo1e (BAKKER, 2003) and is also the range for the model of CHI and NI (2007), except for a small region near the H_2O-$CaCl_2$ binary as described in the text. *Bottom:* The shaded area shows the range of applicability of the model AqSo2e (BAKKER, 2003) and CalcicBrine (NADEN, 1996).

Figure 14. Examples of H_2O-NaCl-$CaCl_2$ fluid inclusion compositions determined from published microthermometric data (sources listed in the legend) using the model developed in this study. Isotherms of measured melting temperatures shown in thin sold lines; pseudobinaries of liquid composition determined from measured cotectic melting temperatures shown as thin dashed lines. See text for description of the data and Table 3 for comparison of the results with those of the original studies.

Figure A1. Example melting pathways, or liquid lines of ascent (up temperature), for select compositions in the H_2O-NaCl-$CaCl_2$ system. *(a)* A fluid with composition "a2" shows first melting at the eutectic (point E, -52°C) where antarcticite is consumed. The liquid composition evolves along the I+HH cotectic until hydrohalite is consumed at point "a1" ($T_{pb,hh}$), after which the liquid evolves toward the H_2O apex until ice is consumed at point "a2" ($T_{m,ice}$), representing the fluid inclusion bulk composition. A fluid with composition "a4" shows hydrohalite melting at the eutectic (point "E") and the liquid evolves along the I+A cotectic until point "a3," ($T_{pb,ant}$) where antarcticite melts, with final melting at point"a4" ($T_{m,ice}$), representing the fluid inclusion bulk composition. *(b)* A fluid of composition "b2" will show the same initial melting sequence as that for composition "a2" except that ice is consumed before hydrohalite on the I+HH cotectic at point "b1" ($T_{pb,ice}$), whereupon the liquid composition evolves directly towards the composition of hydrohalite until $T_{m,hh}$ at point "b2". For composition "b4" ice is lost at the eutectic (point

E) and the liquid composition then evolves along the I+A cotectic until $T_{pb,ant}$ at point "b3" where antarcticite is consumed. The liquid then evolves along a straight line toward the composition of hydrohalite until $T_{m,hh}$ at point "b4". *(c)* For composition "c4" first melting occurs at the eutectic (point "E") where antarcticite is lost. The liquid then evolves along the I+HH cotectic until ice is completely consumed at point "c1" ($T_{pb,ice}$). The liquid composition then evolves directly towards the composition of hydrohalite until the HH+H curve is intersected at point "c2", whereupon halite begins to grow at the expense of hydrohalite, and the liquid composition evolves along the HH+H peritectic curve. Hydrohalite is finally consumed at point "c3" ($T_{pb,hh}$), and the liquid composition then evolves towards the NaCl apex until halite melts at $T_{m,h}$ ("c4"), representing the fluid inclusion bulk composition. Fluid inclusions with composition "c8" follow an analogous pathway, but lose ice at the eutectic (point "E") and next lose antarcticite on the HH+A cotectic at point "c5" ($T_{pb,ant}$). The liquid composition then evolves toward the composition of hydrohalite until the HH+H curve is intersected at point "c6," where halite first nucleates. The liquid composition then evolves along the HH+H curve as halite grows at the expense of hydrohalite with further heating. Hydrohalite is completely consumed at point "c7" ($T_{pb,hh}$), whereupon the liquid composition evolves directly toward the composition of halite until reaching $T_{m,h}$ at point "c8", representing the bulk composition. Fluid inclusions with composition "c10" have first melting at the first ternary peritectic point ("P_1") where hydrohalite is lost, and the liquid evolves along the H+A cotectic until

intersecting the second ternary peritectic point ("P_2"), where a reaction occurs and tetrahydrate grows at the expense of antarcticite by incongruent melting. The liquid composition then evolves along the H+Ca4h cotectic until tetrahydrate is completely consumed at point "c9" ($T_{pb,Ca4h}$). The liquid then evolves towards the NaCl apex until final halite melting at point "c10" ($T_{m,h}$). *(d)* For a fluid inclusion with bulk composition "d2," first melting occurs at the eutectic ("E") where hydrohalite is consumed. The liquid then evolves along the I+A cotectic curve until ice is completely consumed at point "d1" ($T_{pb,ice}$), whereupon the liquid composition evolves directly towards the composition of antarcticite until antarcticite is completely consumed at point "d2" ($T_{m,ant}$). A fluid inclusion with composition "d4" loses ice at the eutectic (point "E"), after which the liquid evolves along the HH+A cotectic until hydrohalite is consumed at point "d3" ($T_{pb,hh}$). The liquid then evolves towards the composition of antarcticite until antarcticite is consumed at point "d4" ($T_{m,ant}$).

Table 1. Summary of the number of published experimental T-X data points for the H_2O-NaCl-$CaCl_2$ system used in this study.

	Solid phase(s) on cotectic and peritectic curves and on liquidus surfaces[a]											
Source	I+HH	I+A	HH+H	HH+A	H+A	H+Ca2h	I	HH	H	A	Ca4h	Ca2h
National Research Council (1928)									19			
Yanatieva (1946)	9	3	6	7	8		57	30	13	20		
Linke (1958)			4		1	2	21	1	57	15	7	12
Potter and Clynne (1978)									11	4	5	5
Vanko et al. (1988)									10			
Oakes et al. (1990)	1						168					
Oakes et al. (1992)	3											
Sterner et al. (1988)									8			
Sub-total							246	31	118	39	12	17
Total[b]	13	3	10	7	9	2	262	61	137	58	12	19

(a) I = ice; HH = hydrohalite; H = halite; A = antarcticite; Ca4h = tetrahydrate; Ca2h = dihydrate

(b) For each one-solid liquidus surface, the total number of data points used in the regression analysis is the sum of the subtotal (data on the one-solid surface) plus the number of data points for the adjacent boundary curves.

Table 2. Coefficients for Equations 1-6.

a_i	Ice (Eqn. 1)	Hydrohalite (Eqn. 2)	Halite (Eqn. 3)	Antarcticite (Eqn. 4)	Tetrahydrate (Eqn. 5)	Dihydrate (Eqn. 6)
a_0	0.46685	0.06039097042	0.0586472647	0.06467408472	1.041627135	0.096475342
a_1	-2.0508125	-2.967800E-5	2.2759389E-4	6.9903747E-4	-0.02232533	1.677838E-3
a_2	-0.08997493	7.0463278E-6	0	-2.607825E-5	1.3792920E-4	-1.3572629E-5
a_3	-2.5468641E-3	1.237133E-3	8.8841217E-9	1.0162876E-6	-2.95841861	4.5571671E-8
a_4	-3.7319837E-5	-1.290978E-3	1.2272697E-3	4.3288357E-9	0.032785047	-0.11534086
a_5	-2.1478861E-7	-5.219129E-3	-3.9989511E-6	1.1648119E-10		
a_6	-1.138304	-3.178747E-6	-6.680437E-9	0.06779525838		
a_7	0.269882	-1.408898E-7	0.0284636532	-1.0833486E-3		
a_8	6.8878422E-3	1.0353807E-3	0			
a_9	1.37774273E-8		3.1094576E-6			

Table 3. Compositions of natural fluid inclusions estimated using the numerical model developed in this study. The compositions reported in the original studies are shown for comparison.

Source	Measured melting temperatures		Salinity		Φ	
			From Source	This Study	From Source	This Study
Layne and Spooner (1991)	$T_{pb,hh}$	$T_{m,ice}$				
	-44.5	-33.5	27	26.5	0.081	0.081
	-49.1	-31.3	26.1	25.6	0.069	0.064
	-49.2	-23.4	23.1	22.3	0.065	0.064
	-49.6	-22.6	22.8	21.9	0.070	0.063
	-45.9	-21.7	22.4	21.5	0.076	0.075
	-46.6	-19.3	21.2	20.3	0.075	0.072
	-43.7	-18.0	20.3	19.7	0.079	0.085
	-46.5	-18.0	20.4	19.6	0.069	0.073
	-45.6	-17.5	20	19.4	0.075	0.076
	-47.2	-14.2	17.9	17.4	0.073	0.070
Nyman et al. (1990)	$T_{pb,ice}$	$T_{m,hh}$				
	-41.0 to -25.0	-9.6 to -7.0	26 to 27	26.4 to 30.4	0.6 to 0.7	0.16 to 0.63
Vanko et al. (1988)	$T_{c,ice}$	$T_{m,h}$				
	-30.9	+278	41	39.7	0.74	0.70
	-34.8	+402	51.3	50.7	0.87	0.85
	-29.9	+288	41.5	40.1	0.76	0.72
	-30.8	+286	41.5	40.2	0.75	0.71
Schiffries (1990) –"Type 1"	$T_{pb,ant}$	$T_{m,h}$				
	+22 to +29	+161 to +201	-	46.5 to 50.3	-	0.15 to 0.24
Schiffries (1990) –"Type 3"	$T_{pb,Ca4h}$	$T_{m,h}$				
	+31 to +38	+173 to +225	-	49.8 to 53.9	-	0.14 to 0.25

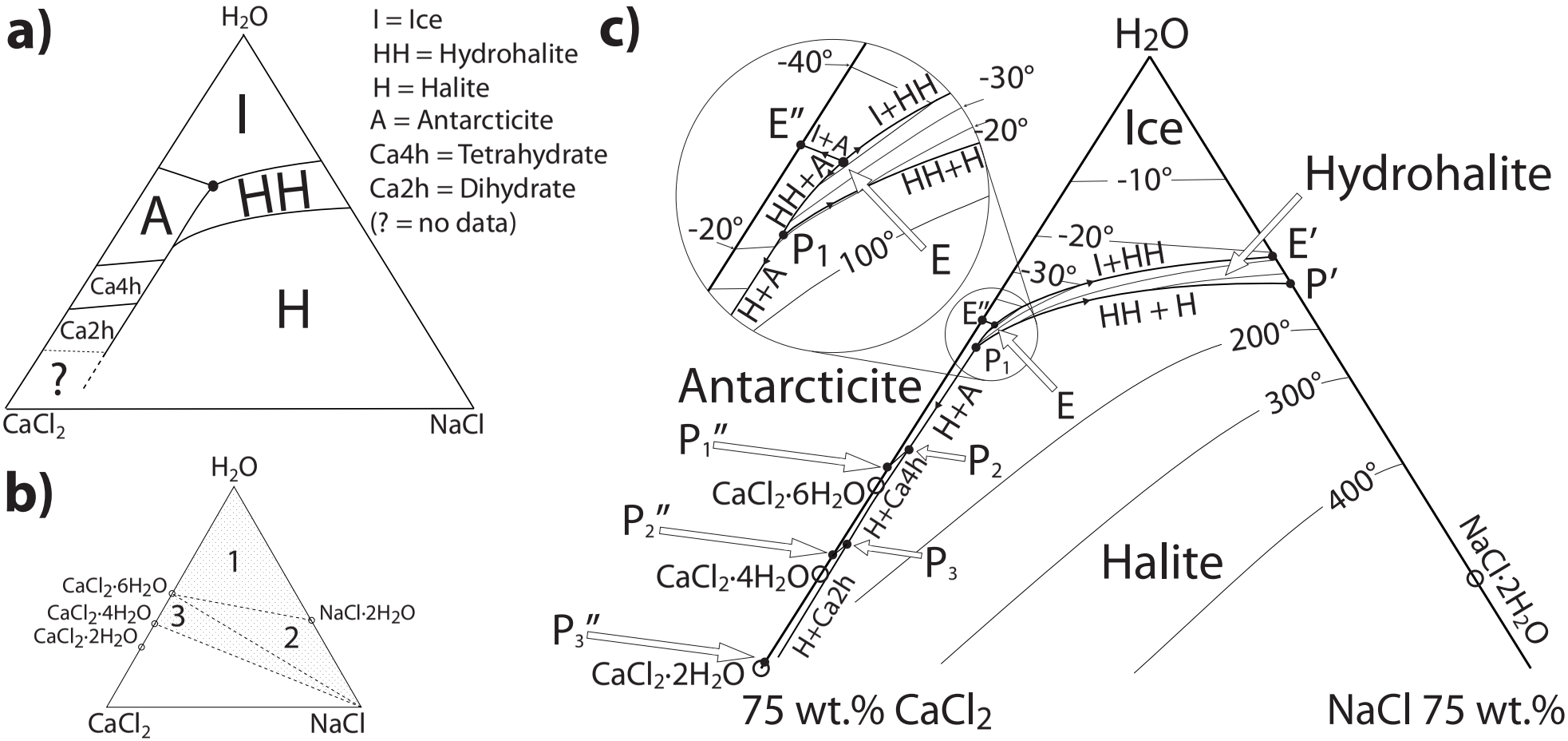
a)
H2O
I
HH
A
H
Ca4h
Ca2h
?
CaCl2
NaCl
I = Ice
HH = Hydrohalite
H = Halite
A = Antarcticite
Ca4h = Tetrahydrate
Ca2h = Dihydrate
(? = no data)
b)
H2O
1
2
3
CaCl2·6H2O
CaCl2·4H2O
CaCl2·2H2O
NaCl·2H2O
CaCl2
NaCl
c)
H2O
Ice
Hydrohalite
Antarcticite
Halite
-40°
-30°
-20°
-10°
100°
200°
300°
400°
E″
E′
P′
P1
E
I+HH
I+A
HH+A
HH+H
H+A
HH + H
P1″
P2
P2″
P3
P3″
CaCl2·6H2O
CaCl2·4H2O
CaCl2·2H2O
H+Ca4h
H+Ca2h
NaCl·2H2O
75 wt.% CaCl2
NaCl 75 wt.%

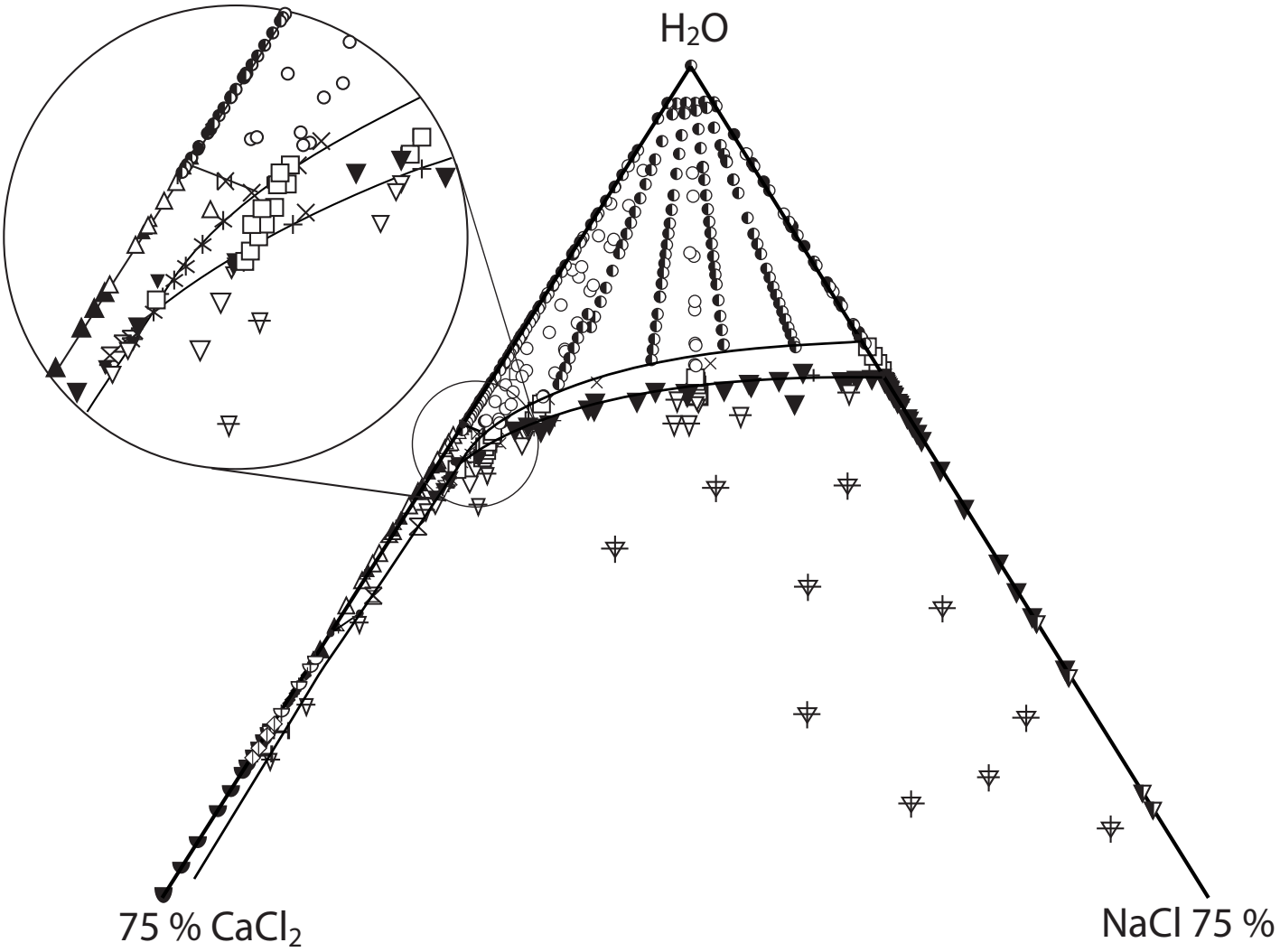

Source	I+HH	HH+H	I+A	HH+A	H+A	H+Ca2h	I	H	HH	A	Ca4h	Ca2h
National Reseach Council (1928)								▽				
Yanatieva (1946)	×	+	⋈	∗	⧖		○	▽	□	△		
Linke (1958)		+			⧖	⊢	●	▼	■	▲	◆	◒
Potter and Clynne (1978)								▽		◭	◇	◒
Vanko et al. (1988)								▽				
Oakes et al. (1990)	×						◐					
Oakes et al. (1992)	×											
Sterner et al. (1988)								▼				

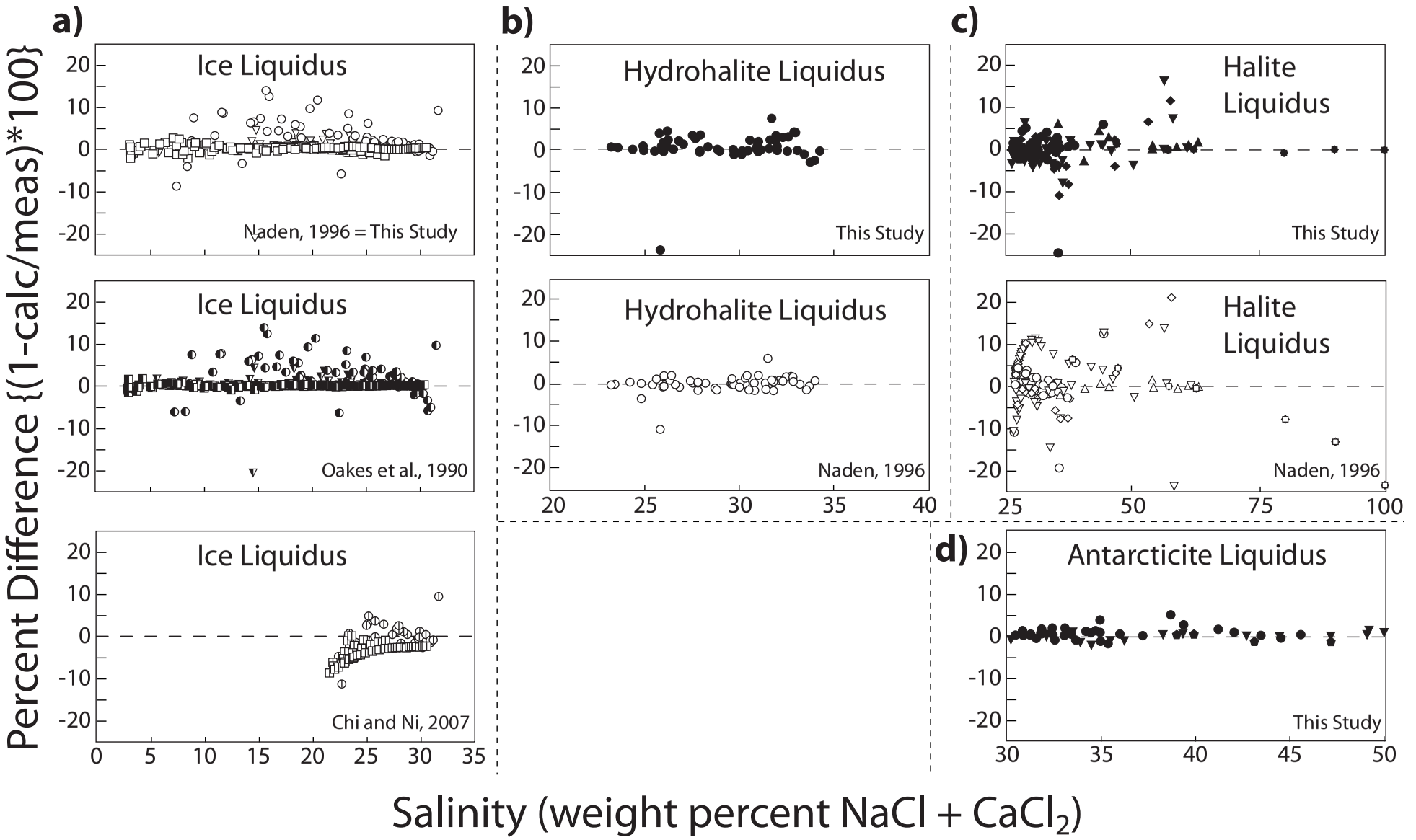
a)
Ice Liquidus
Naden, 1996 = This Study
Ice Liquidus
Oakes et al., 1990
Ice Liquidus
Chi and Ni, 2007
b)
Hydrohalite Liquidus
This Study
Hydrohalite Liquidus
Naden, 1996
c)
Halite Liquidus
This Study
Halite Liquidus
Naden, 1996
d)
Antarcticite Liquidus
This Study
Percent Difference {(1-calc/meas)*100}
Salinity (weight percent NaCl + CaCl2)

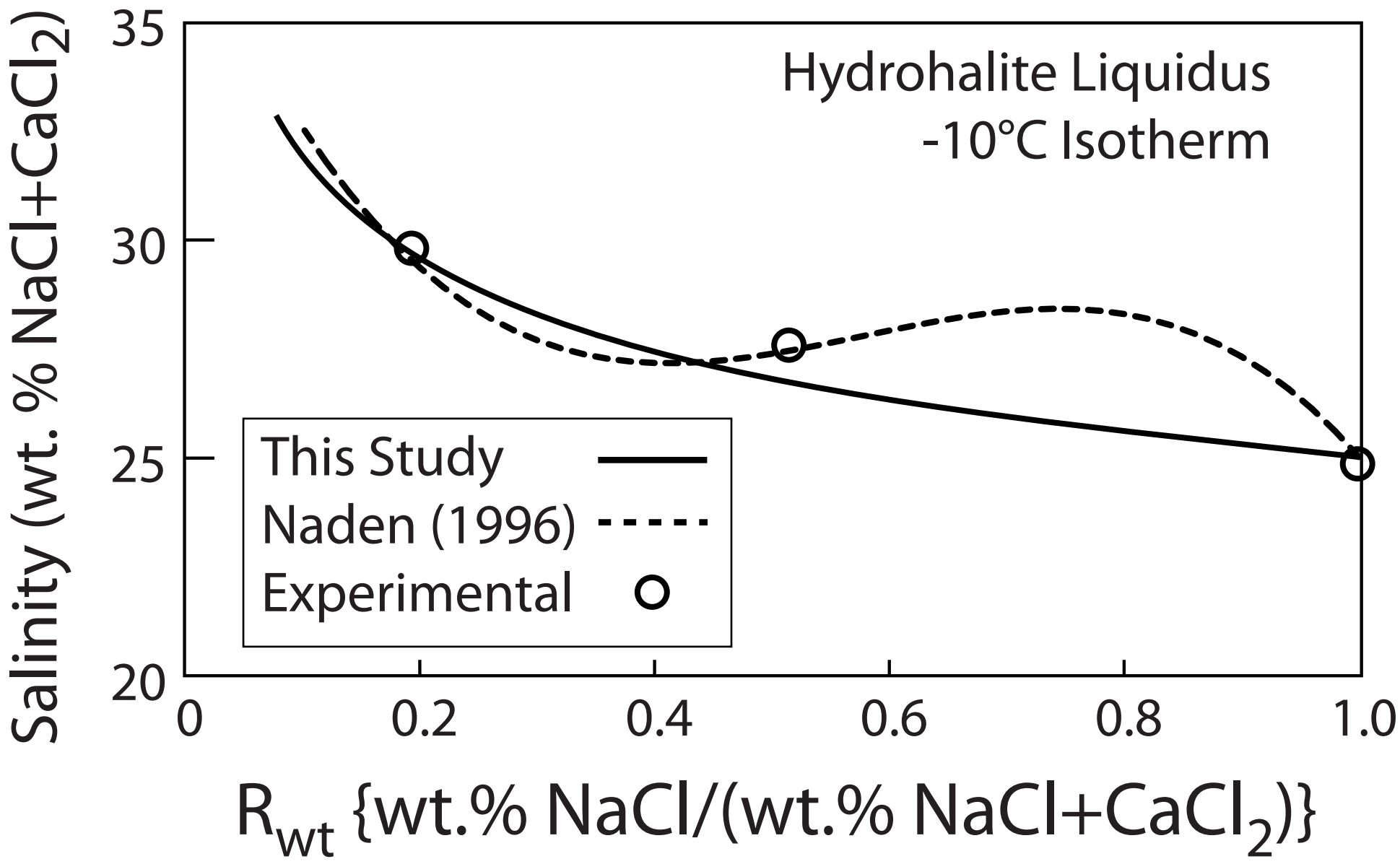
Hydrohalite Liquidus
-10°C Isotherm
This Study
Naden (1996)
Experimental
Salinity (wt. % NaCl+CaCl2)
35
30
25
20
0
0.2
0.4
0.6
0.8
1.0
Rwt {wt.% NaCl/(wt.% NaCl+CaCl2)}

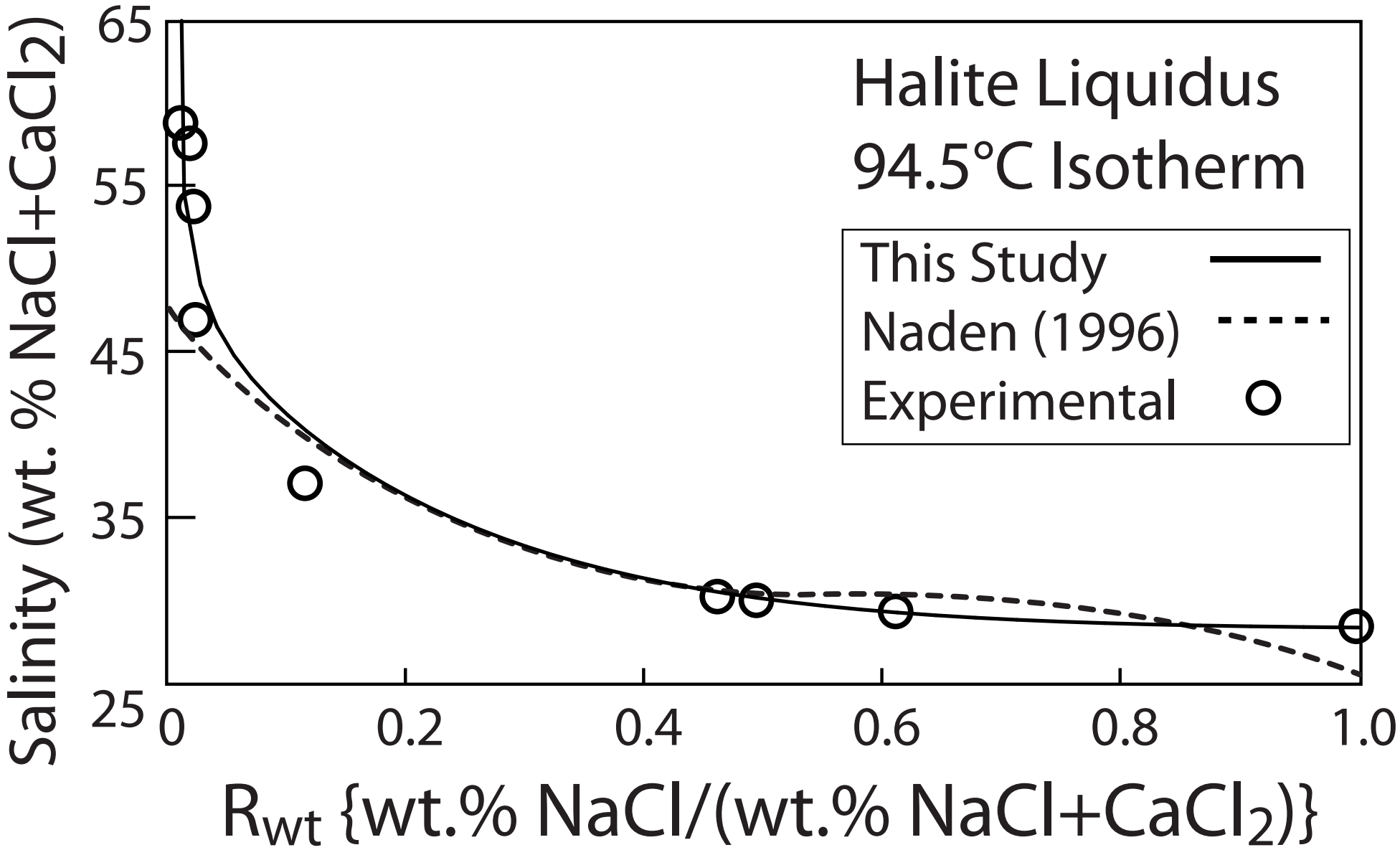
Halite Liquidus
94.5°C Isotherm
This Study
Naden (1996)
Experimental
Salinity (wt. % NaCl+CaCl2)
65
55
45
35
25
0
0.2
0.4
0.6
0.8
1.0
Rwt {wt.% NaCl/(wt.% NaCl+CaCl2)}

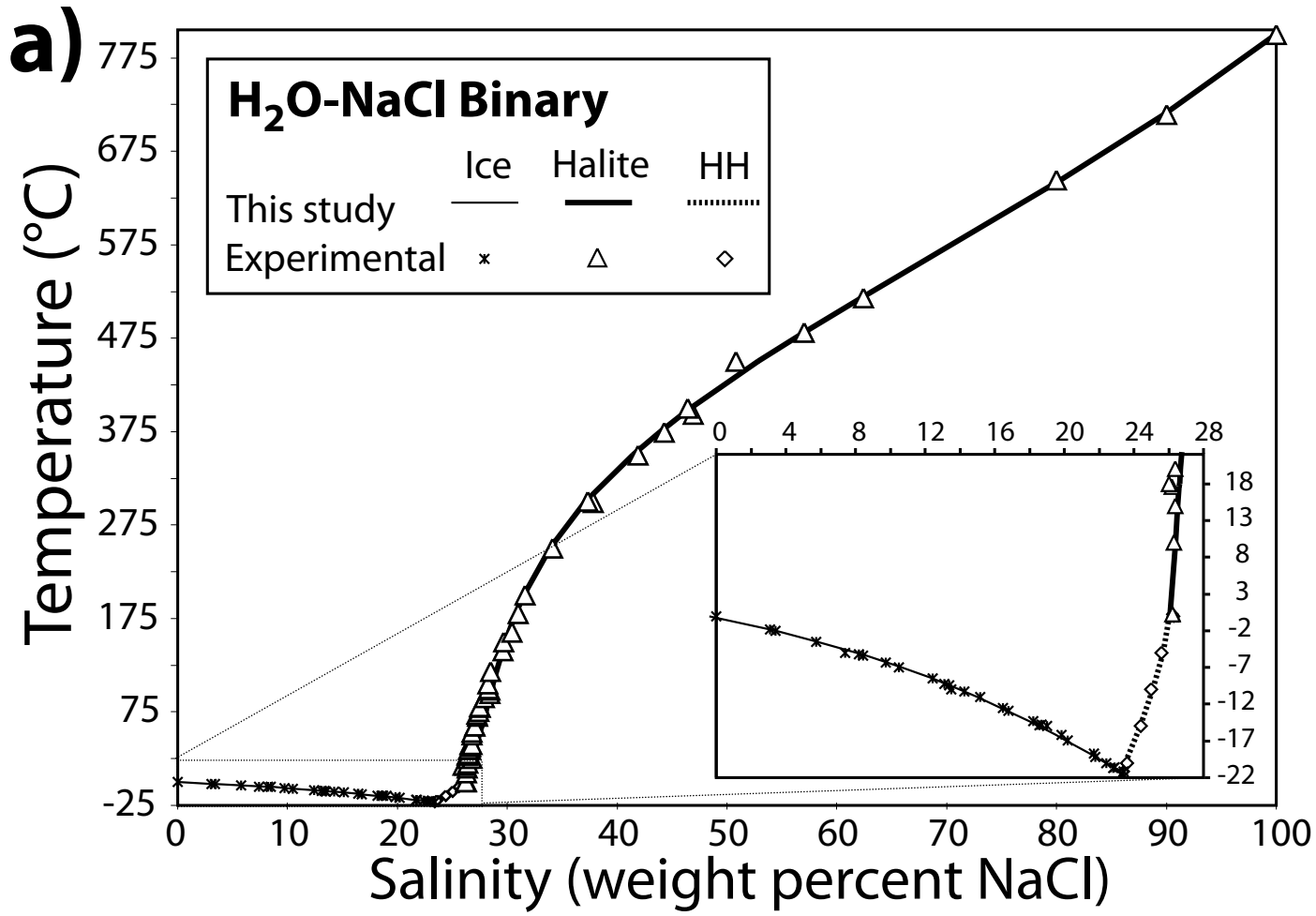
a)
H2O-NaCl Binary
Ice
Halite
HH
This study
Experimental
Temperature (°C)
775
675
575
475
375
275
175
75
-25
0
10
20
30
40
50
60
70
80
90
100
Salinity (weight percent NaCl)
0
4
8
12
16
20
24
28
18
13
8
3
-2
-7
-12
-17
-22

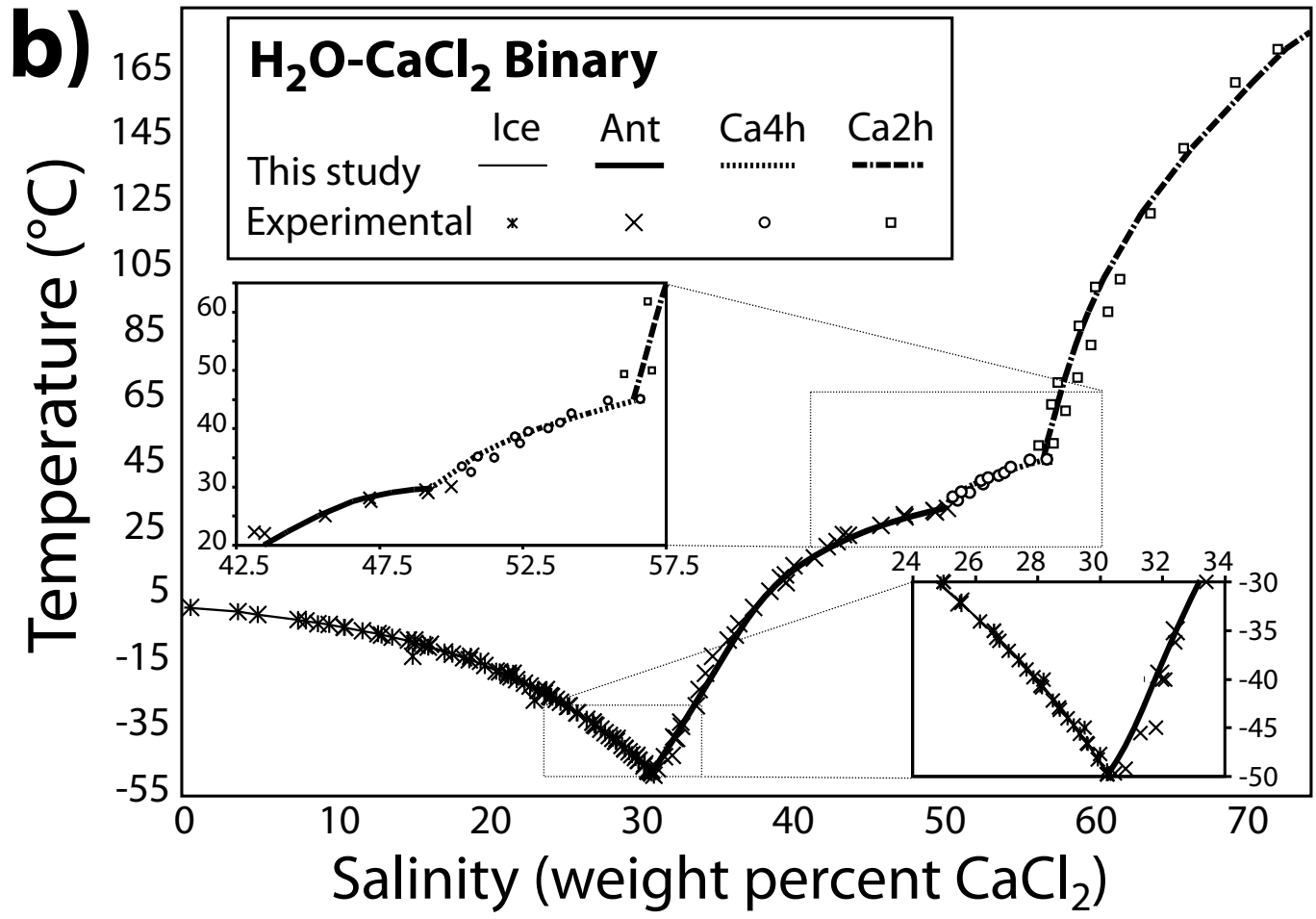
b)
H2O-CaCl2 Binary
Ice
Ant
Ca4h
Ca2h
This study
Experimental
Temperature (°C)
165
145
125
105
85
65
45
25
5
-15
-35
-55
0
10
20
30
40
50
60
70
Salinity (weight percent CaCl2)
60
50
40
30
20
42.5
47.5
52.5
57.5
24
26
28
30
32
34
-30
-35
-40
-45
-50

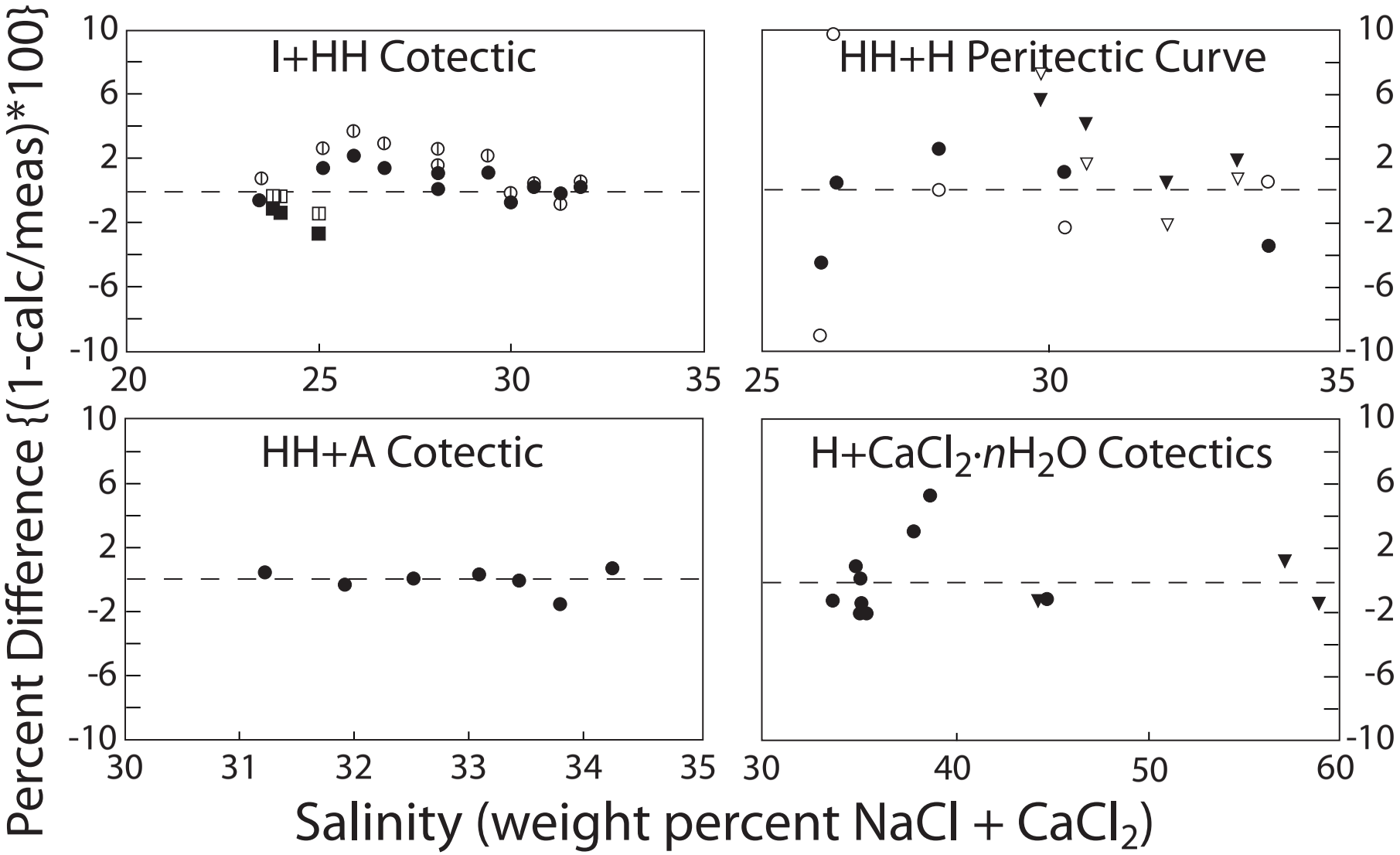
I+HH Cotectic
HH+H Peritectic Curve
HH+A Cotectic
H+CaCl2·nH2O Cotectics
Percent Difference {(1-calc/meas)*100}
Salinity (weight percent NaCl + CaCl2)
10
6
2
-2
-6
-10
20
25
30
35
31
32
33
34
40
50
60

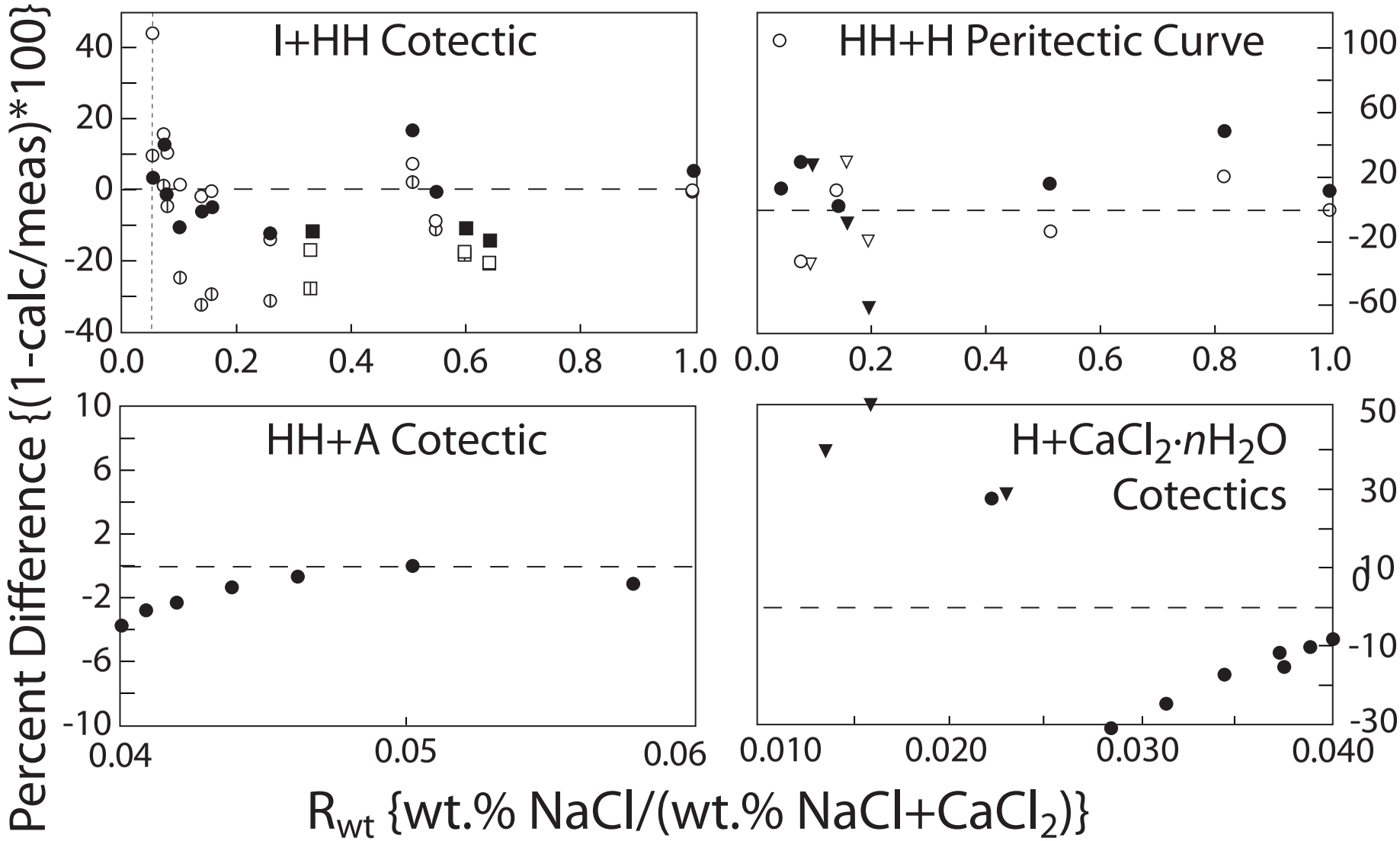
I+HH Cotectic
HH+H Peritectic Curve
HH+A Cotectic
H+CaCl2·nH2O
Cotectics
Percent Difference {(1-calc/meas)*100}
Rwt {wt.% NaCl/(wt.% NaCl+CaCl2)}

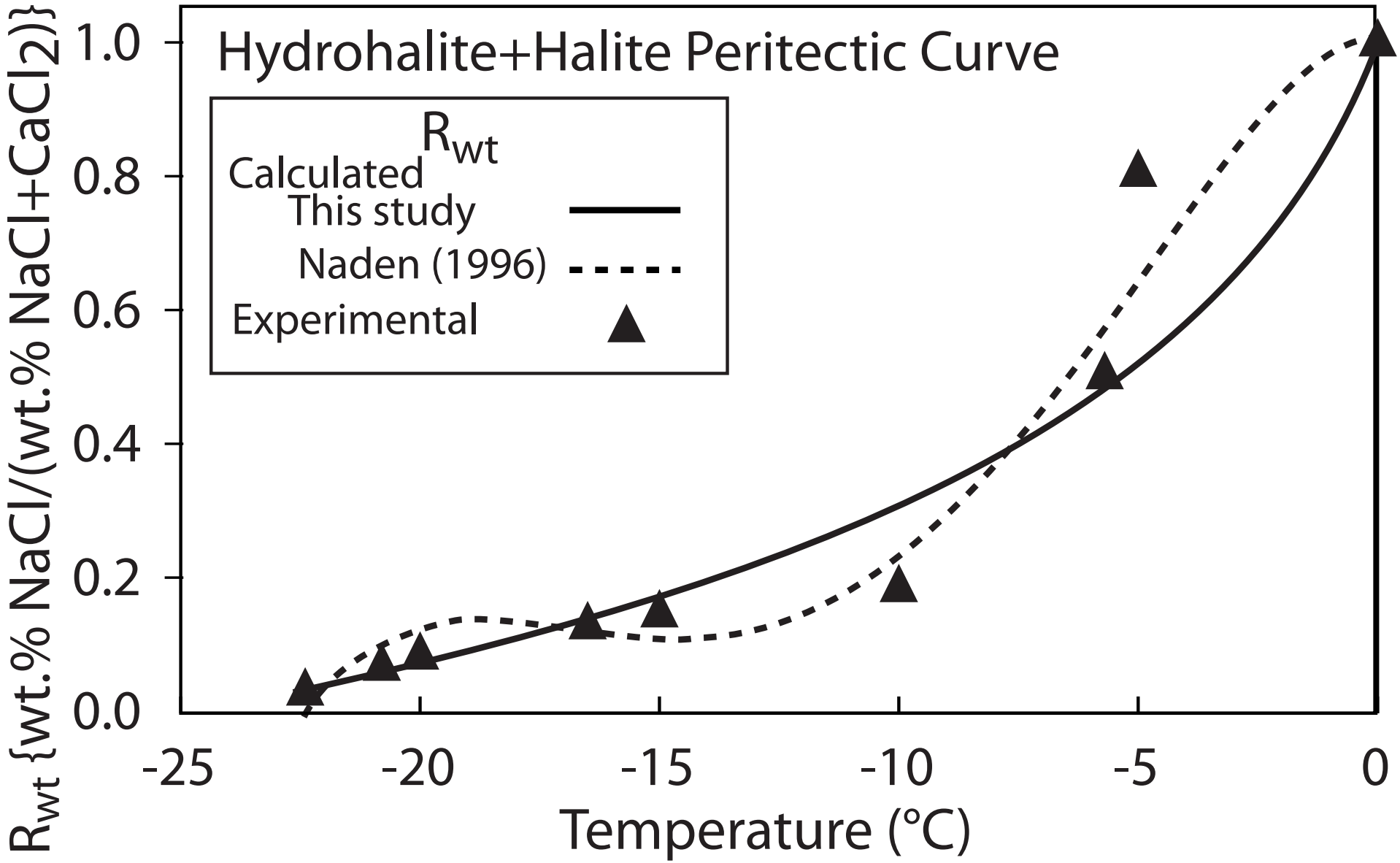
Hydrohalite+Halite Peritectic Curve
R_{wt}
Calculated
This study
Naden (1996)
Experimental
R_{wt} {wt.% NaCl/(wt.% NaCl+CaCl2)}
1.0
0.8
0.6
0.4
0.2
0.0
-25
-20
-15
-10
-5
0
Temperature (°C)

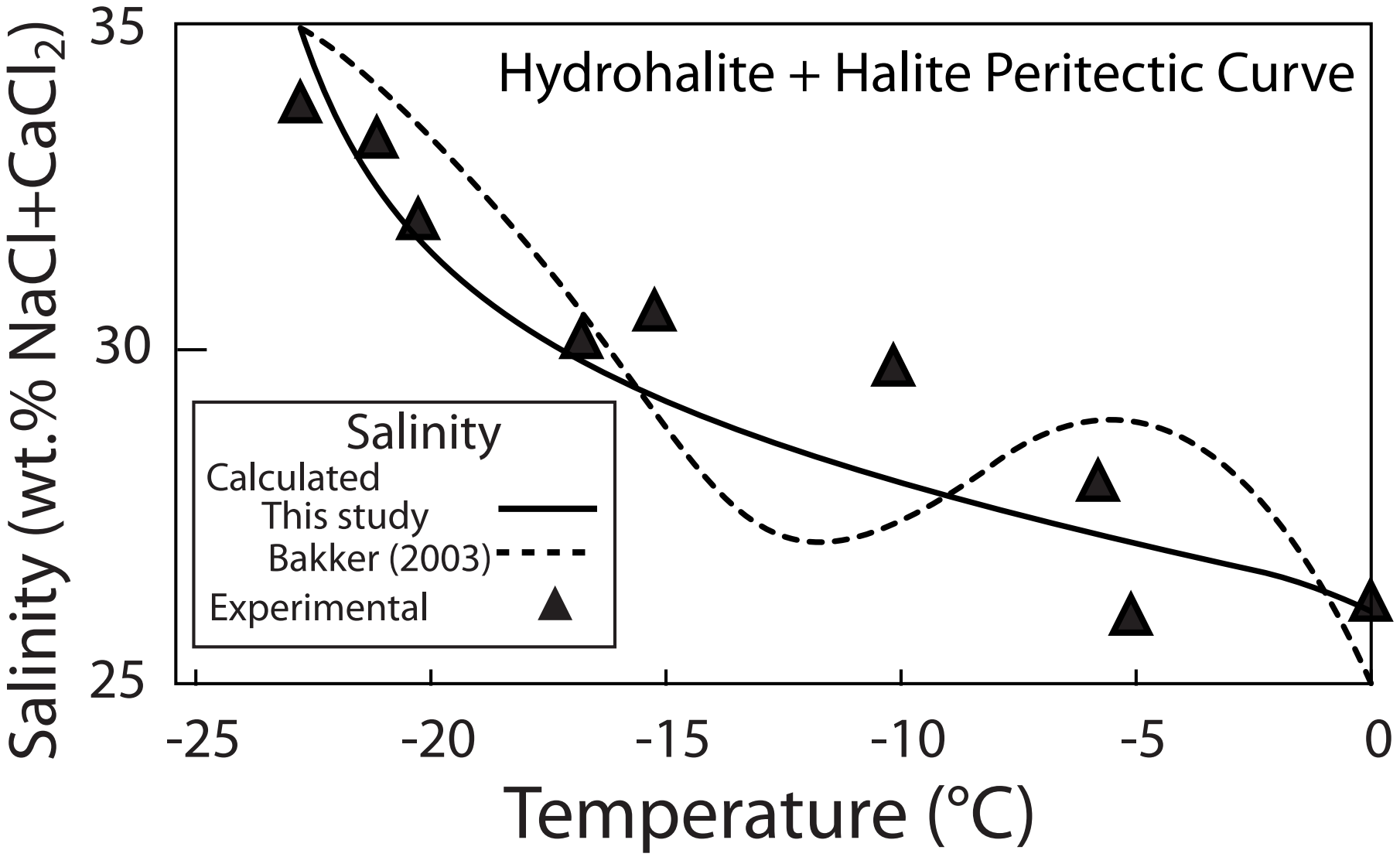
Hydrohalite + Halite Peritectic Curve
Salinity
Calculated
This study
Bakker (2003)
Experimental
Salinity (wt.% NaCl+CaCl2)
35
30
25
-25
-20
-15
-10
-5
0
Temperature (°C)

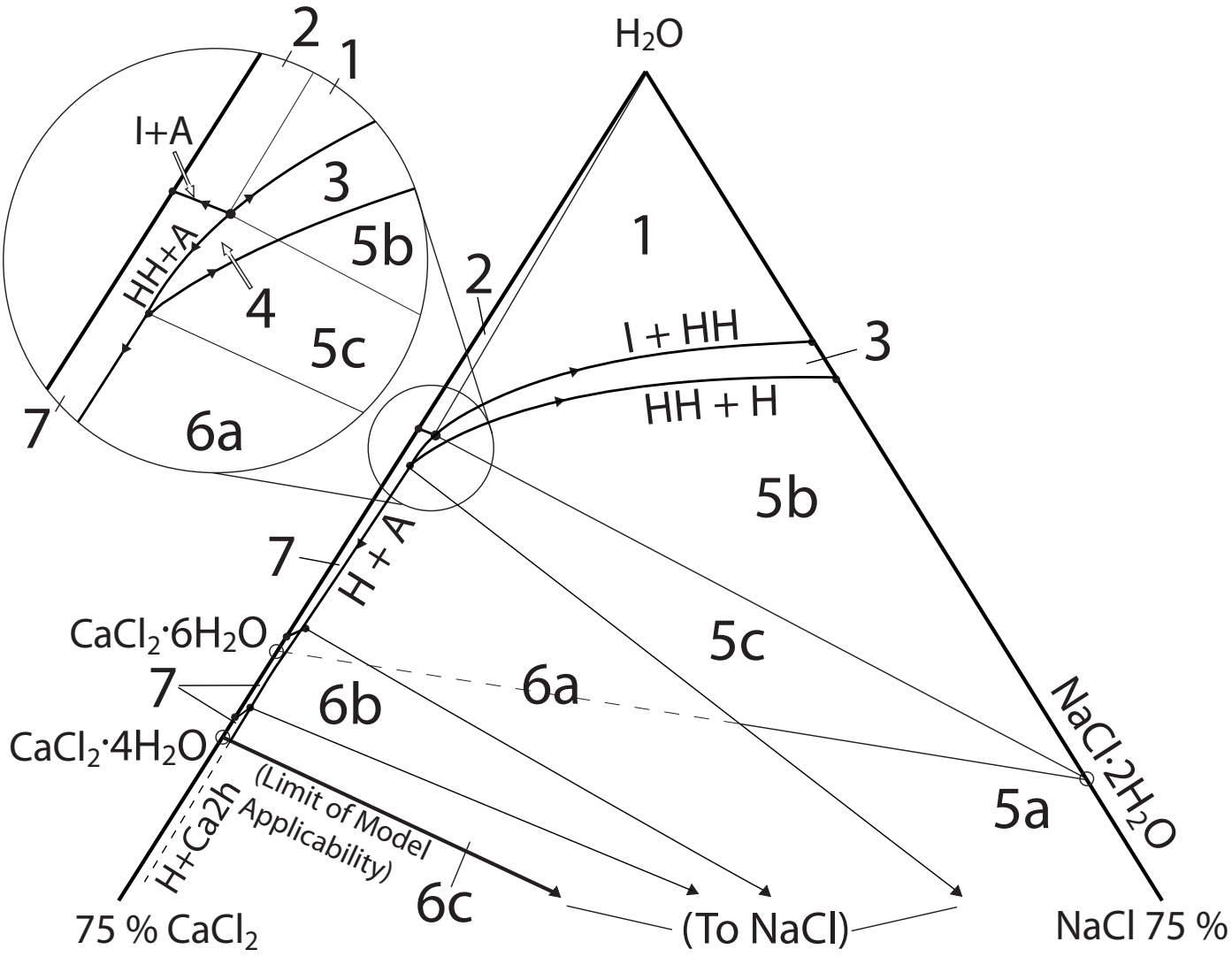
2
1
I+A
3
HH+A
5b
4
5c
7
6a
H2O
1
2
I + HH
3
HH + H
5b
7
H + A
5c
CaCl2·6H2O
7
6a
6b
CaCl2·4H2O
NaCl·2H2O
5a
H+Ca2h
(Limit of Model Applicability)
6c
75 % CaCl2
(To NaCl)
NaCl 75 %

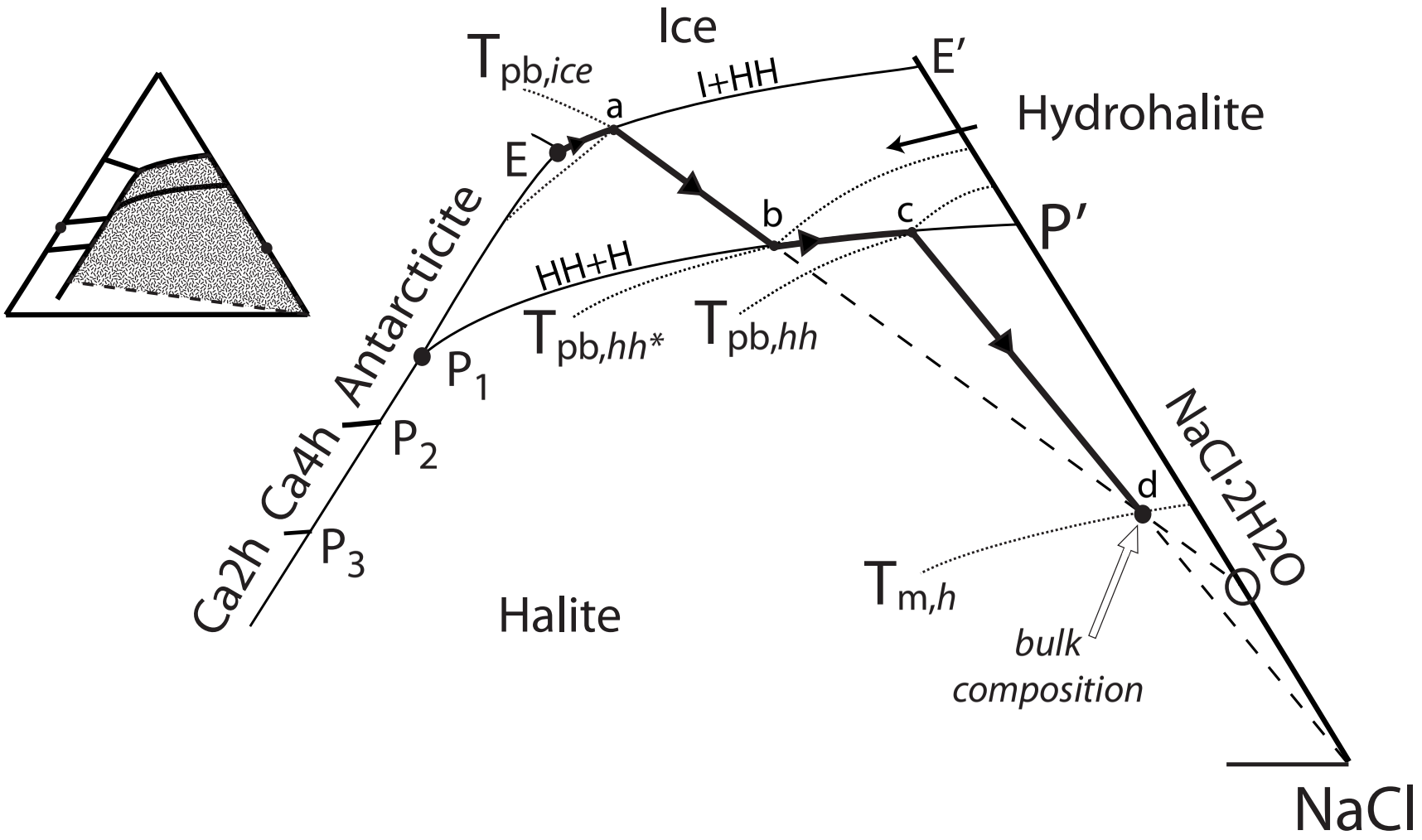
Ice
$T_{pb,ice}$
E′
I+HH
a
Hydrohalite
E
b
c
P′
HH+H
$T_{pb,hh*}$
$T_{pb,hh}$
P_1
Antarcticite
P_2
Ca4h
Ca2h
P_3
NaCl·2H2O
d
$T_{m,h}$
Halite
bulk
composition
NaCl

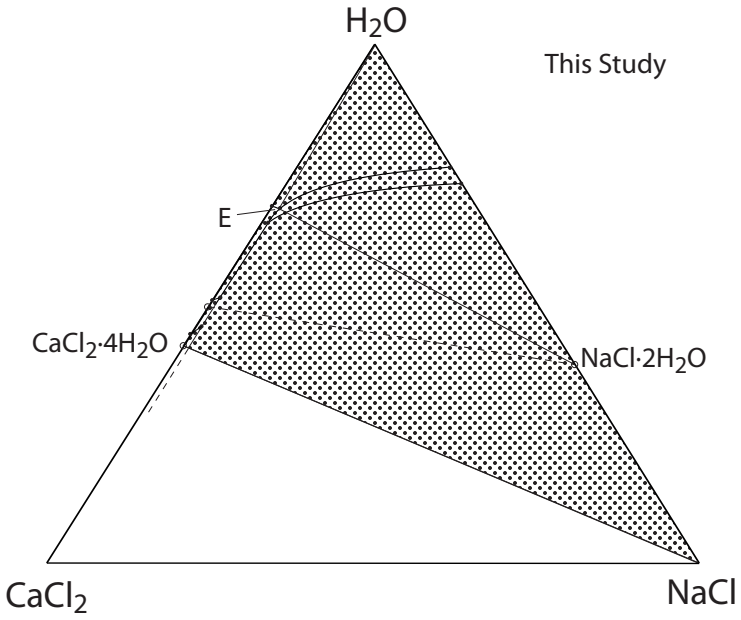
H_2O
This Study
E
$CaCl_2{\cdot}4H_2O$
$NaCl{\cdot}2H_2O$
$CaCl_2$
NaCl

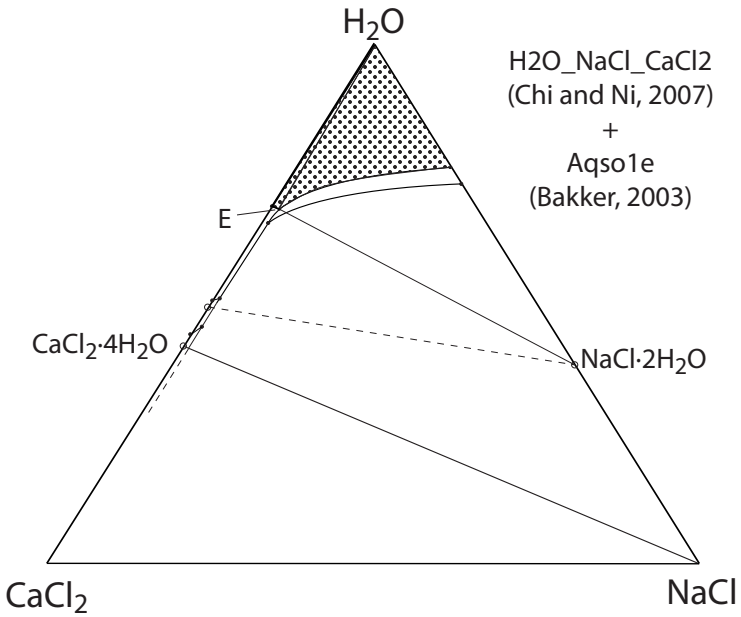
H_2O
H2O_NaCl_CaCl2
(Chi and Ni, 2007)
+
Aqso1e
(Bakker, 2003)
E
$CaCl_2{\cdot}4H_2O$
$NaCl{\cdot}2H_2O$
$CaCl_2$
NaCl

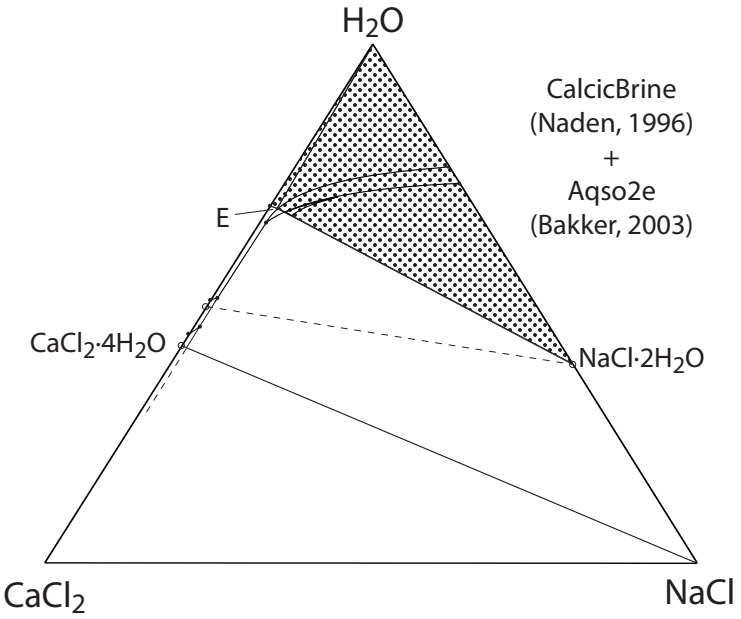
H_2O
CalcicBrine
(Naden, 1996)
+
Aqso2e
(Bakker, 2003)
E
$CaCl_2{\cdot}4H_2O$
$NaCl{\cdot}2H_2O$
$CaCl_2$
NaCl

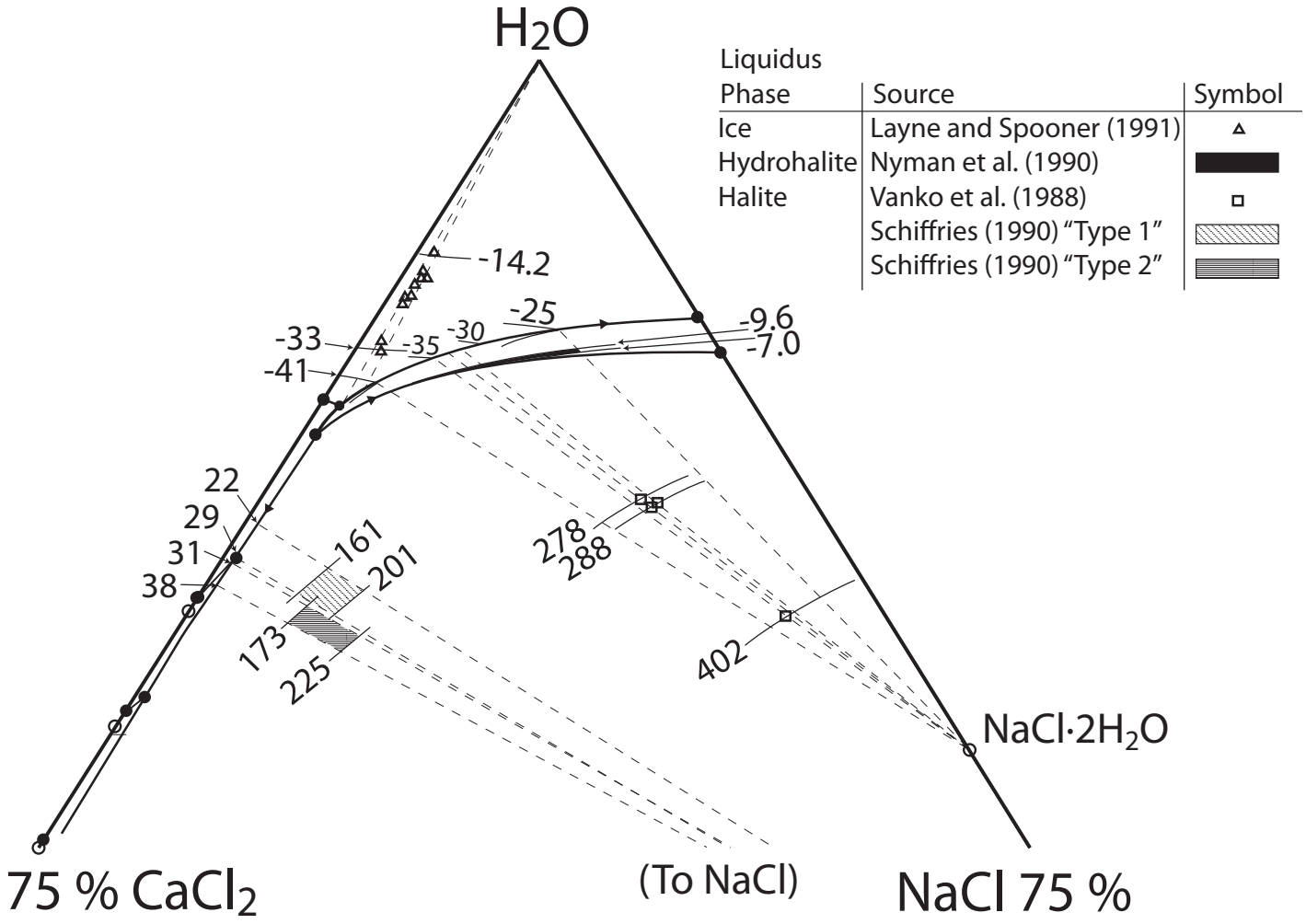
H2O
Liquidus
Phase
Source
Symbol
Ice
Layne and Spooner (1991)
Hydrohalite
Nyman et al. (1990)
Halite
Vanko et al. (1988)
Schiffries (1990) "Type 1"
Schiffries (1990) "Type 2"
-14.2
-25
-9.6
-7.0
-33
-35
-30
-41
22
29
31
38
161
201
173
225
278
288
402
NaCl·2H2O
75 % CaCl2
(To NaCl)
NaCl 75 %

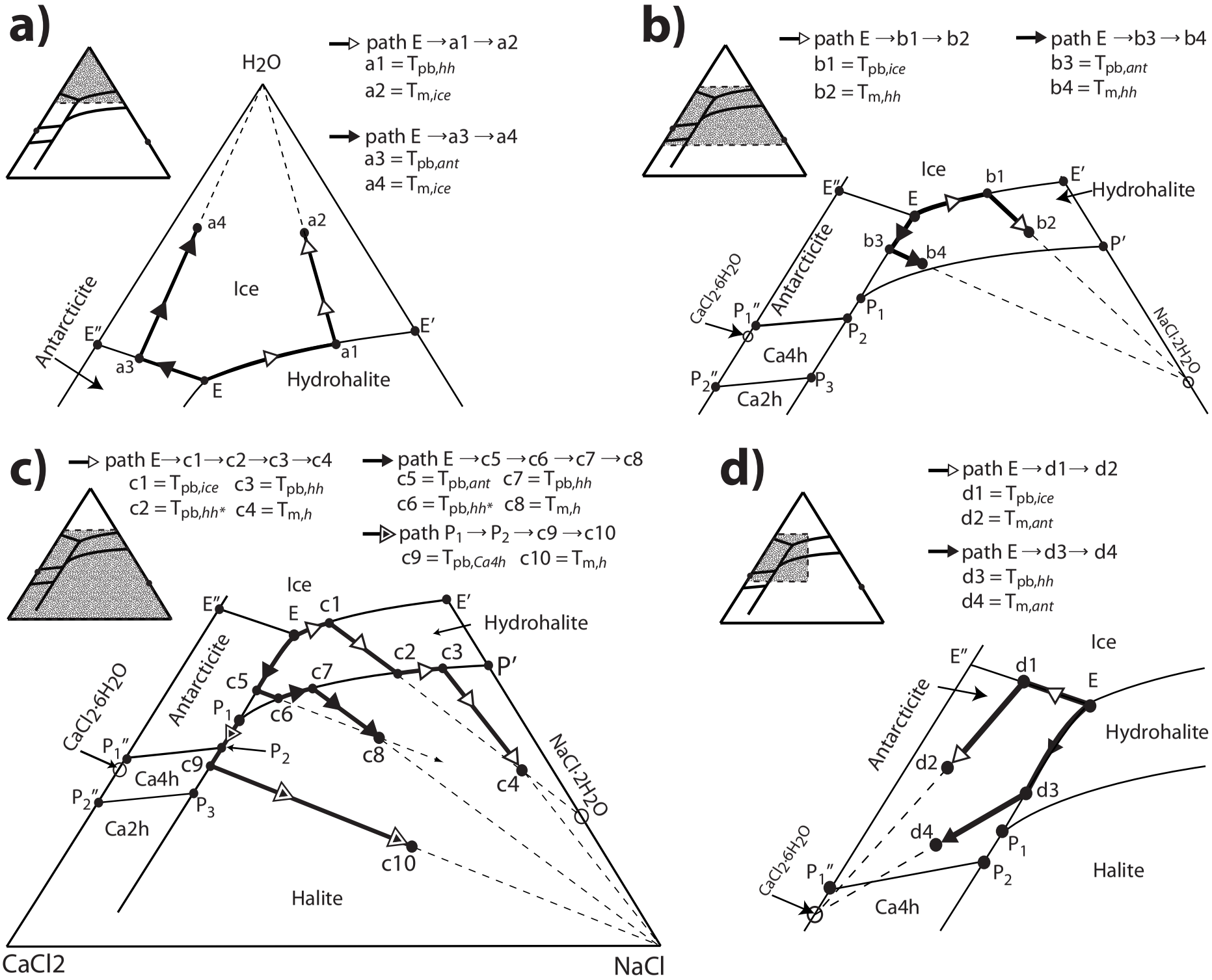
a)
H2O
path E → a1 → a2
a1 = Tpb,hh
a2 = Tm,ice
path E → a3 → a4
a3 = Tpb,ant
a4 = Tm,ice
a4
a2
Ice
Antarcticite
E″
a3
E
a1
E′
Hydrohalite
b)
path E → b1 → b2
b1 = Tpb,ice
b2 = Tm,hh
path E → b3 → b4
b3 = Tpb,ant
b4 = Tm,hh
Ice
E″
E
b1
E′
Hydrohalite
b2
b3
b4
P′
CaCl2·6H2O
Antarcticite
P1″
P1
P2
NaCl·2H2O
Ca4h
P2″
P3
Ca2h
c)
path E → c1 → c2 → c3 → c4
c1 = Tpb,ice c3 = Tpb,hh
c2 = Tpb,hh* c4 = Tm,h
path E → c5 → c6 → c7 → c8
c5 = Tpb,ant c7 = Tpb,hh
c6 = Tpb,hh* c8 = Tm,h
path P1 → P2 → c9 → c10
c9 = Tpb,Ca4h c10 = Tm,h
Ice
E″
E
c1
E′
Hydrohalite
c2
c3
P′
c5
c7
c6
P1
CaCl2·6H2O
Antarcticite
P1″
P2
c8
NaCl·2H2O
c9
Ca4h
c4
P2″
P3
Ca2h
c10
Halite
CaCl2
NaCl
d)
path E → d1 → d2
d1 = Tpb,ice
d2 = Tm,ant
path E → d3 → d4
d3 = Tpb,hh
d4 = Tm,ant
Ice
E″
d1
E
Antarcticite
Hydrohalite
d2
d3
d4
P1
CaCl2·6H2O
P1″
P2
Halite
Ca4h